Title: Flexible coordinator and switcher hubs for adaptive task control

Abbreviated title: Flexible coordinator and switcher hubs

Authors: Carrisa V Cocuzza (corresponding author)[1,2], Takuya Ito[1,2], Douglas Schultz[1,3], Danielle S Bassett[4], Michael W Cole[1]

[1]Center for Molecular and Behavioral Neuroscience, Rutgers University, Newark, NJ, USA, 07102
[2]Behavioral and Neural Sciences PhD Program, Rutgers University, Newark, NJ, USA, 07102
[3]Center for Brain Biology and Behavior, University of Nebraska-Lincoln, Lincoln, NE, USA, 68588
[4]Departments of Bioengineering, Physics & Astronomy, Electrical & Systems Engineering, and Neurology, University of Pennsylvania, Philadelphia, PA, USA, 19104

Corresponding author: Carrisa V Cocuzza, Center for Molecular and Behavioral Neuroscience, Rutgers University, 197 University Avenue, Newark, NJ 07102, carrisacocuzza@gmail.com

Conflict of Interest: The authors declare no competing financial interests.

Acknowledgments: This project was supported by the US National Institutes of Health, under awards K99-R00 MH096901 and R01 MH109520. The content is the sole responsibility of the authors and does not necessarily represent the official views of any of the funding agencies. The authors acknowledge the Office of Advanced Research Computing (OARC) at Rutgers, The State University of New Jersey for providing access to the Amarel cluster and associated research computing resources. The authors thank their colleagues at the Cole Neurocognition Lab and the Rutgers University Brain Imaging Center (RUBIC) for their expertise and diligent efforts in data collection, as well as offering words of wisdom and overall support.

Keywords: cognitive control, network dynamics, executive function, network interactions, cognitive flexibility, task representation

Abstract

Functional connectivity studies have identified at least two large-scale neural systems that constitute cognitive control networks – the frontoparietal network (FPN) and cingulo-opercular network (CON). Control networks are thought to support goal-directed cognition and behavior. It was previously shown that the FPN flexibly shifts its global connectivity pattern according to task goal, consistent with a "flexible hub" mechanism for cognitive control. Our aim was to build on this finding to develop a functional cartography (a multi-metric profile) of control networks in terms of dynamic network properties. Here, we report that large-scale network interactions in the FPN and CON are critical to flexible task representation in (male and female) humans using a high-control-demand cognitive paradigm involving switching among 64 task sets. Further, we quantified functional properties of these network interactions across task sets. We hypothesized that cognitive control is enacted by the FPN and CON via distinct but complementary roles reflected in network dynamics. Consistent with a flexible "coordinator" mechanism, FPN connections were varied across tasks, while maintaining within-network connectivity to aid cross-region coordination. Consistent with a flexible "switcher" mechanism, CON regions switched to other networks in a task-dependent manner, driven primarily by reduced within-network connections to other CON regions. This pattern of results suggests FPN acts as a dynamic, global coordinator of goal-relevant information, while CON transiently disbands to lend processing resources to other goal-relevant networks. This cartography of network dynamics reveals a dissociation between two prominent cognitive control networks, suggesting complementary mechanisms underlying goal-directed cognition.

Significance Statement

Cognitive control supports a variety of behaviors requiring flexible cognition, such as rapidly switching between tasks. Furthermore, cognitive control is negatively impacted in a variety of mental illnesses. We used tools from network science to characterize the implementation of cognitive control by large-scale brain systems. This revealed that two systems – the frontoparietal (FPN) and cingulo-opercular (CON) networks – have distinct but complementary roles in controlling global network reconfigurations. The FPN exhibited properties of a flexible coordinator (orchestrating task changes), while CON acted as a flexible switcher (switching specific regions to other systems to lend processing resources). These findings reveal an underlying distinction in cognitive processes that may be applicable to clinical, educational, and machine learning work targeting cognitive flexibility.

Introduction

Theories of cognitive control – processes supporting goal-directed cognition and behavior – suggest the need for flexibly reconfigurable neural systems to support controlled processing (Desimone and Duncan, 1995; Miller and Cohen, 2001; Schneider and Chein, 2003; Cole et al., 2013). In order for an individual's goals to be implemented, goal-relevant information must be appropriately represented across large-scale neural systems, or networks. Importantly, goals and goal-relevant information are subject to change over time (such as sensorimotor information that corresponds to changing task conditions). Processing these dynamic changes must be guided amongst neural systems that represent goal-relevant information. Cognitive control networks

are proposed to enact this guidance via network interactions that are flexible with respect to the current task context (Waskom et al., 2014). Thus, we focus here on the role of large-scale network dynamics as task goals are updated across 64 systematically-related task contexts demanding high levels of cognitive control (Fig. 1).

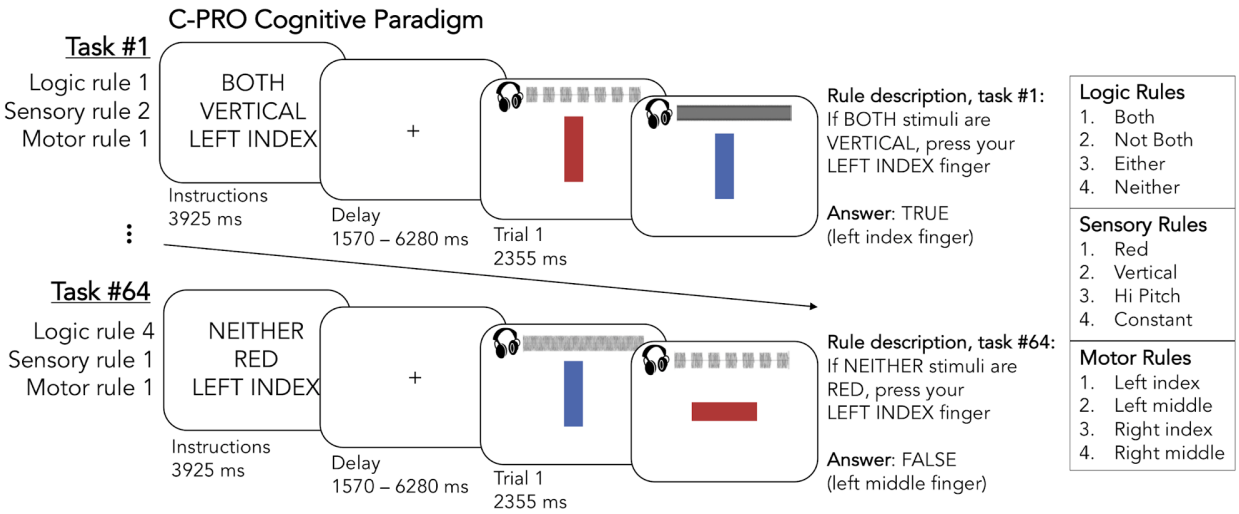

Figure 1. The Concrete Permuted Rule Operations (C-PRO) cognitive paradigm. First, an instruction screen presented the rules for a given task (3925 ms). Participants next applied these rules to pairs of consecutively presented audiovisual stimuli (auditory waveforms are visually depicted here, but were only presented audibly to participants). Two example task-rule sets are depicted, as well as how participants were trained to interpret the rules (e.g., rule descriptions on the right-most portion of panel A) (see Materials and Methods for details). The 12 possible rules are listed on the right.

The theoretical insight that large-scale network interactions are essential to cognitive control evolved over the last several decades, beginning with empirical observations (e.g., Fuster et al., 1985), which then led to the biased competition theory (Desimone et al., 1990; Desimone and Duncan, 1995). This theory focused on lateral prefrontal cortex influencing the visual system by biasing its competition for attentional resources toward goal-relevant representations. Building on the biased competition theory, the guided activation theory generalized this prefrontal network mechanism to all task domains. This theory proposed a general role for top-down prefrontal influences in accomplishing task goals (Miller and Cohen, 2001). More recently, the flexible hub theory generalized the guided activation theory beyond prefrontal cortex to the entire frontoparietal network (FPN) and formalized the importance of cross-network, global connectivity changes in implementing cognitive control (Cole et al., 2013b). The present study builds on this to further verify and expand the flexible hub theory.

Simultaneous with these advances in theory have been observations of a second major neural system supporting cognitive control: the cingulo-opercular network (CON). Like the FPN, the CON is active as a function of cognitive control demands across a wide variety of tasks (Dosenbach et al., 2006; Yeo et al., 2015; Crittenden et al., 2016). However, CON and FPN are not equally active for all task conditions and they maintain distinct functional network architectures in terms of resting-state functional connectivity (rsFC) (Dosenbach et al., 2007; Power et al., 2011; Ji et al., 2019) and task-state functional connectivity (tFC) (Cole et al., 2014). Moreover, the

specific functional contributions of CON regions have not been fully established, with some studies suggesting that CON regions specify overall task set modes of processing (Dosenbach et al., 2007; Sadaghiani and D'Esposito, 2015), and others emphasizing the CON's role in reactive (phasic) attention (Seeley et al., 2007), and relatedly, conflict processing (Botvinick, 2007; Cole et al., 2009; Braem et al., 2019). Ultimately, unlike the FPN, the relationship between the CON and the flexible hub theory (and the theories it builds upon) remains unclear.

The present study builds on our prior work demonstrating flexible hub properties in FPN regions, expanding on the characterization of these FPN network mechanisms, while also investigating CON network mechanisms. We previously found that FPN's global tFC patterns flexibly updated according to task demands more than any other network, including CON (Cole et al., 2013b). However, given that large-scale network dynamics are central to cognitive control, and given that both the CON and FPN contain hubs (Power et al., 2011; Ito et al., 2017), we hypothesized that CON reflects flexible hub properties in addition to FPN. Unlike FPN's continuous goal-coordinating role, we expected CON to exhibit a more discrete network switching mechanism, reflecting its proposed role in specifying overall task-set modes of processing (Dosenbach et al., 2007; Sadaghiani and D'Esposito, 2015). Consistent with this, we found that FPN regions act as "flexible coordinators" and CON regions as "flexible switchers", providing separate but complementary network mechanisms in support of cognitive control (Fig. 2).

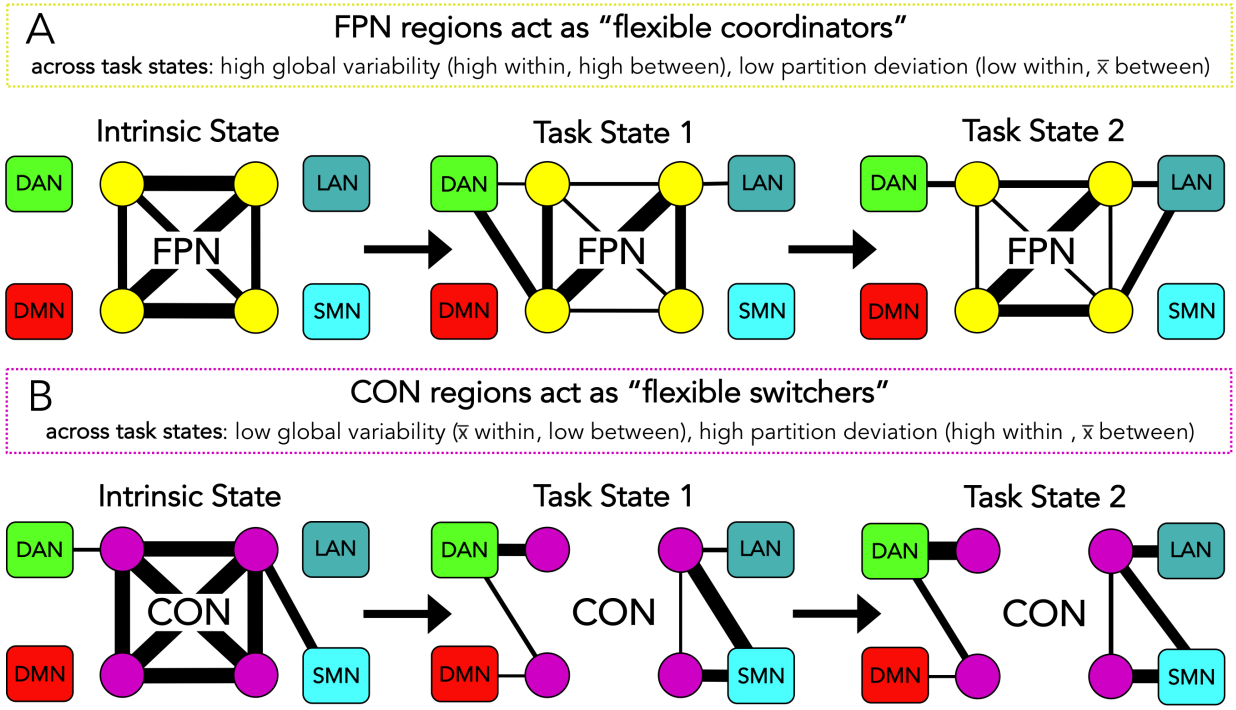

Figure 2. Schematic depictions of cognitive control network functional properties (see Materials and Methods and Results for details on network measures). In each panel, a "toy" version of the control network is prominently depicted in the center (with a reduced number of regions, or nodes, and simplified within-network connections), and out-of-network exemplars are depicted as truncated and surrounding the control network of interest (*DAN*: dorsal attention network, *LAN*: language network, *DMN*: default mode network, and *SMN*: somatomotor network). Each of these surrounding networks also contains within-network regions and connections (not depicted here for

simplicity). (***A***) Regions in the frontoparietal network (FPN) acted as flexible coordinators. This entailed high global variability and low partition deviation across task states. From example task state one to task state two, FPN regions maintain their within-network connectivity (low deviation) and out-of-network connectivity changes are variable across states (high GVC). (See Results for details). (***B***) Regions in the cingulo-opercular network (CON) acted as flexible switchers. This entails low global variability and high partition deviation. From example task state one to task state two, CON regions drop their within-network connectivity (high deviation) and out-of-network connectivity changes are consistent across states (low GVC). (See Results for details).

Materials and Methods

Participants

Right-handed, healthy adult participants (N=106) were recruited from Rutgers University and the surrounding Newark, New Jersey community. Six participants were excluded from analyses due to technical errors, leaving a total sample size of N=100 (see Extended Data Tables 1-1 and 1-2 for demographic data). To improve replicability, we used a split-sample validation approach (Anderson and Magruder, 2017) with a random subset of n=50 comprising a discovery dataset and the remaining n=50 comprising a replication dataset. All participants provided informed consent in accordance with protocols approved by the Institutional Review Board of Rutgers University-Newark. Each participant provided or completed the following: (1) demographic information and intake survey questions, (2) the National Institutes of Health Cognition Toolbox (Gershon et al., 2013), including a neuropsychological battery, (3) behavioral training on the C-PRO task (outside the scanner), (4) resting-state fMRI, and (5) C-PRO task fMRI. The subsets of data assessed herein included (1), (4), and (5) (see Schultz et al., 2019 for assessment of other variables). There were no significant differences between identified genders on the distributions of age, ethnicity, or education (Extended Data Table 1-1 and 1-2).

Concrete Permuted Rule Operations (C-PRO) paradigm

The C-PRO paradigm was designed to involve rapid instructed task learning (RITL) through compositionally combining various task rules (Cole et al., 2010, 2013a; Ito et al., 2017). This further provided a high demand on cognitive control across all C-PRO task states. We used a modified version of the PRO paradigm from Cole et al. (2010), which was previously introduced by Ito et al. (2017) (Fig. 1). This paradigm permutes rules across three domains: four logic rules (both, not both, either, and neither), four sensory rules (red color, vertical orientation, high pitch sound, and constant tone), and four motor rules (left index, right index, left middle, and right middle fingers). This amounts to 12 rule sets represented 16 times across 64 unique task states. The software for presenting the task was E-Prime version 2.0.10.353 (Schneider et al., 2002).

In each task state, an initial instruction screen was presented for 3925 ms for participants to memorize a given permuted rule set (Fig. 1). This was followed by a jittered delay (1570 – 6280 ms, randomized from a uniform distribution), then three trials of paired audiovisual stimuli for participants to adjudicate based upon the given rule set (2355 ms each trial; inter-trial interval of 1570 ms). Another jittered delay occurred at the end of each task state (7850 – 12560 ms, randomized), which was immediately followed by the next permuted rule set instruction screen. An example instruction screen (Fig. 1; task state one) read: “BOTH, VERTICAL, LEFT INDEX”, indicating: “If both stimuli are vertical, press your left index finger”. In each of the three trials

that followed, participants judged if both paired stimuli were vertically oriented, and either pressed the left index finger button to indicate "true" or the left middle finger button to indicate "false" (a judgement of "false" was always the same hand but opposite finger). Importantly, stimuli were always presented with auditory and visual features concurrently. Thus, focusing on the sensory rule given by the instructions was paramount (i.e., "VERTICAL" indicated that one should ignore auditory information, color information, and only focus on line orientation). Additionally, participants were required to remember and apply conditional logic and nontrivial motor commands each trial. Altogether this multitask behavioral paradigm is condition-rich and necessitates ongoing cognitive control.

Each participant completed a training session outside the scanner and a testing session within the scanner (task-state fMRI) 30 minutes later. During the training session participants equally practiced four rule sets that contained all 12 rules. This practice set was counterbalanced amongst participants and supplementary instruction was provided for training purposes (e.g., use the same hand but opposite finger to indicate "false"). Task fMRI scans were performed in eight runs, altogether containing 64 task state miniblocks, twice over (e.g., 128 task miniblocks), with each block composed of a permuted rule set (Fig. 1). Each task fMRI run was approximately eight minutes in duration, and identical miniblocks were never presented consecutively. Overall, mean performance was 83.47% correct (SD=9.00%). There was no significant difference in performance (percent correct) between males (M=83.65%, SD=10.44%) and females (M=83.33%, SD=7.80%); $t(74.71)=0.17$, $p=0.87$.

Study design and statistical analysis

Participants were randomly allocated to either a discovery dataset (n=50) or replication dataset (n=50). The replication dataset was not analyzed until after analyses of the discovery dataset were complete. Analyses of replication data were identical to analyses of discovery data (using the same code, including all chosen parameters), and additionally included measures of similarity between replication and discovery results to quantify expected generalizability (Anderson and Magruder, 2017).

Whenever multiple comparisons were addressed, we utilized the Max-T nonparametric permutation testing approach (10,000 permutations) with maxima-derived 95% confidence intervals for statistical hypothesis testing against zero (Blair and Karniski, 1993; Nichols and Holmes, 2002). To analyze the similarity of two correlation (weighted adjacency) matrices we used the Mantel permutation test, which performs a Pearson's correlation across the upper triangles (off-diagonal) of the matrices (Mantel, 1967; Glerean et al., 2016). The Mantel test is more conservative than a standard comparison between connectivity matrices because it takes into account the fact that observations in distance/similarity matrices are not independent (an assumption of both parametric and standard non-parametric tests). In each Mantel analysis, we again used nonparametric permutation procedures to derive statistics that make minimal assumptions about probability distribution (10,000 permutations unless otherwise specified). Henceforth we will describe these matrix similarity statistics as Mantel-r.

MRI parameters

All MRI data were collected at the Rutgers University Brain Imaging Center (RUBIC). When possible, the best practices suggested by the Human Connectome Project preprocessing pipelines were followed (Glasser et al., 2013). A 3T, 32-channel head coil within a Siemens Trio scanner was used to obtain multiband, whole-brain, and echo-planar imaging (EPI). The repetition time (TR) was 785 ms; the echo time (TE) was 34.8 ms; the flip angle was 55°; the bandwidth was 1924 Hz/Px; the in-plane field-of-view (FoV) read was 208 mm; 72 slices; 2.0 mm isotropic voxels; and the multiband acceleration factor was 8. Whole-brain and high-resolution T1-weighted and T2-weighted anatomical scans were also acquired, with an isotropic voxel resolution of 0.8 mm. Spin echo field maps were obtained in both the anterior-posterior and posterior-anterior directions. Resting-state fMRI scans were 14 minutes in duration, amounting to 1070 TRs. Each task (i.e., C-PRO) fMRI run was approximately eight minutes in duration, adding up to approximately one hour in the scanner for the task session (36 TRs per task miniblock; 4608 TRs altogether).

fMRI preprocessing

The open-source Human Connectome Project minimal preprocessing pipeline (Glasser et al., 2013), version 3.5.0, was applied to all neuroimaging data. This included: anatomical reconstruction and segmentation; EPI reconstruction, segmentation, and spatial normalization to a standard template; intensity normalization; and motion correction. The resulting data was in CIFTI 64k-vertex grayordinate space, and all subsequent analyses were performed in MATLAB R2014b (The Mathworks, Inc.). Following minimal preprocessing, vertices were parcellated into 360 cortical regions (180 per hemisphere) per the Glasser et al. (2016) atlas. To parcellate each of these regions, we calculated the average time series of enclosed vertices.

Next, we performed nuisance regression on parcellated resting-state and task-state data using 6 motion parameters plus their derivatives (totaling 12 motion parameters), and volumetrically-extracted ventricle and white matter timeseries (via FreeSurfer http://surfer.nmr.mgh.harvard.edu/), plus their first derivatives (16 regressors overall). Note that global signal was not removed due to evidence that it can artificially introduce negative relationships (Murphy et al., 2009). Task time series were further processed to account for confounding effects introduced by simultaneous sensory inputs (e.g., left and right primary visual area, V1) and their downstream effects by fitting a general linear model (GLM) to task activity estimated by a finite impulse response (FIR) function. This removal of cross-event mean task-locked activity has been shown to reduce task-evoked correlation false positives while retaining most (approximately 90%) of the correlated variance between fMRI time series and without inflating false negatives (Cole et al., 2019). In the task GLM, each task run was separately demeaned, and drift was accounted for with a per-run linear trend.

Functional connectivity estimation

Functional connectivity (FC) was estimated for parcellated (region-wise), pre-processed data, per participant and per state (one resting state and 64 C-PRO task states). Across the whole cortex, we utilized Fisher's Z-transformed Pearson correlation coefficients to compute interregional relationships of blood-oxygen-level dependent (BOLD) timeseries, resulting in 360 by 360 connectivity matrices. Given the complex nature of subsequent analyses (i.e., network metrics)

we chose this method of FC estimation for simplicity and wide-reaching comprehension. In the present study, connectivity estimates tended to decrease from rest to task, a finding that has been observed across numerous prior studies (that utilized various model species and neural recording methods) (Cohen and Maunsell, 2009; He, 2013; Cole et al., 2014; Ponce-Alvarez et al., 2015) and has well-founded neural mechanisms (Ito et al., 2019).

Network partition

We applied the cortical portion of the Cole-Anticevic brain-wide network partition (CAB-NP) (Ji et al., 2019; Fig. 4C and Extended Data Fig. 4-1), which was based on publicly available Human Connectome Project data. The CAB-NP was based on resting-state fMRI data across the whole brain, and used the Louvain community detection algorithm to assign parcellated cortical regions (Glasser et al., 2016) into 12 functional networks. The CAB-NP corroborated features of well-known cortical partitions (Power et al., 2011; Yeo et al., 2011; Gordon et al., 2016), yet found novel but robust networks. The CAB-NP was implemented for all analyses except network flexibility, which requires the application of community detection (Louvain Q-modularity; see Materials and Methods section below on network flexibility).

Given that our novel network metric (see Materials and Methods section on network partition deviation) quantifies network affiliation changes from an intrinsic partition, it was important (in order to avoid inflated deviation estimates) to ensure that the intrinsic partition was applicable to the present group of subjects. We first partitioned resting-state data by sorting regional FC estimates per the 12 CAB-NP network indices. We then found the maximum FC estimate (i.e., the intrinsic "preference") for each region (per participant), and tested if its location was equivalent to the CAB-NP. If this index was different from the CAB-NP in over 50% of participants, we reassigned that region to its empirically-derived preference. We henceforth used this empirically-adjusted CAB-NP to sort task-state data into networks (see Extended Data Fig. 4-1).

In select analyses, we probed the similarity of two partitions. To accomplish this, we used the Jaccard index, which is a standard measure of similarity from set theory. For example, the Jaccard index was used to assess the similarity of the empirically-adjusted resting-state partitions of the discovery and replication datasets. We used the MATLAB *jaccard* function, which utilized the "intersection over union" formula on label vectors A and B, with the following equation:

$$jaccard(A,B) = |intersection(A,B)|/|union(A,B)|$$

Per state, the intersection equaled the number of true positives (i.e., overlap of two partitions), and the union was the number of true positives summed with the number of false positives and false negatives.

Network metrics

Interregional connectivity was probed by three network metrics for state-based reconfiguration properties (Medaglia et al., 2015): (1) Global variability coefficient (GVC; Cole et al., 2013b, and relatedly, between-network variability coefficient (BVC; novel but related to Ito et al., 2017), (2) Network flexibility (NF; Bassett et al., 2011, 2013a), and (3) Network partition deviation (deviation; novel). Network metrics were computed across states and averaged across regions that compose a given network, per participant. In analyses that used standardized metrics (i.e.,

z-scores), standardizations were performed before network averages and standard errors were computed. Figure 3 illustrates the algorithms of these metrics schematically. Table 1 summarizes the primary characteristics of these metrics, including formulae, interpretations, parameter-space considerations, and reliance on a predefined network partition. A predefined network partition is sometimes called a “hard partition”, and refers to the use of a predefined network or community assignment structure, such that each parcellated region is indexed into the partition *a priori* (Sporns and Betzel, 2016).

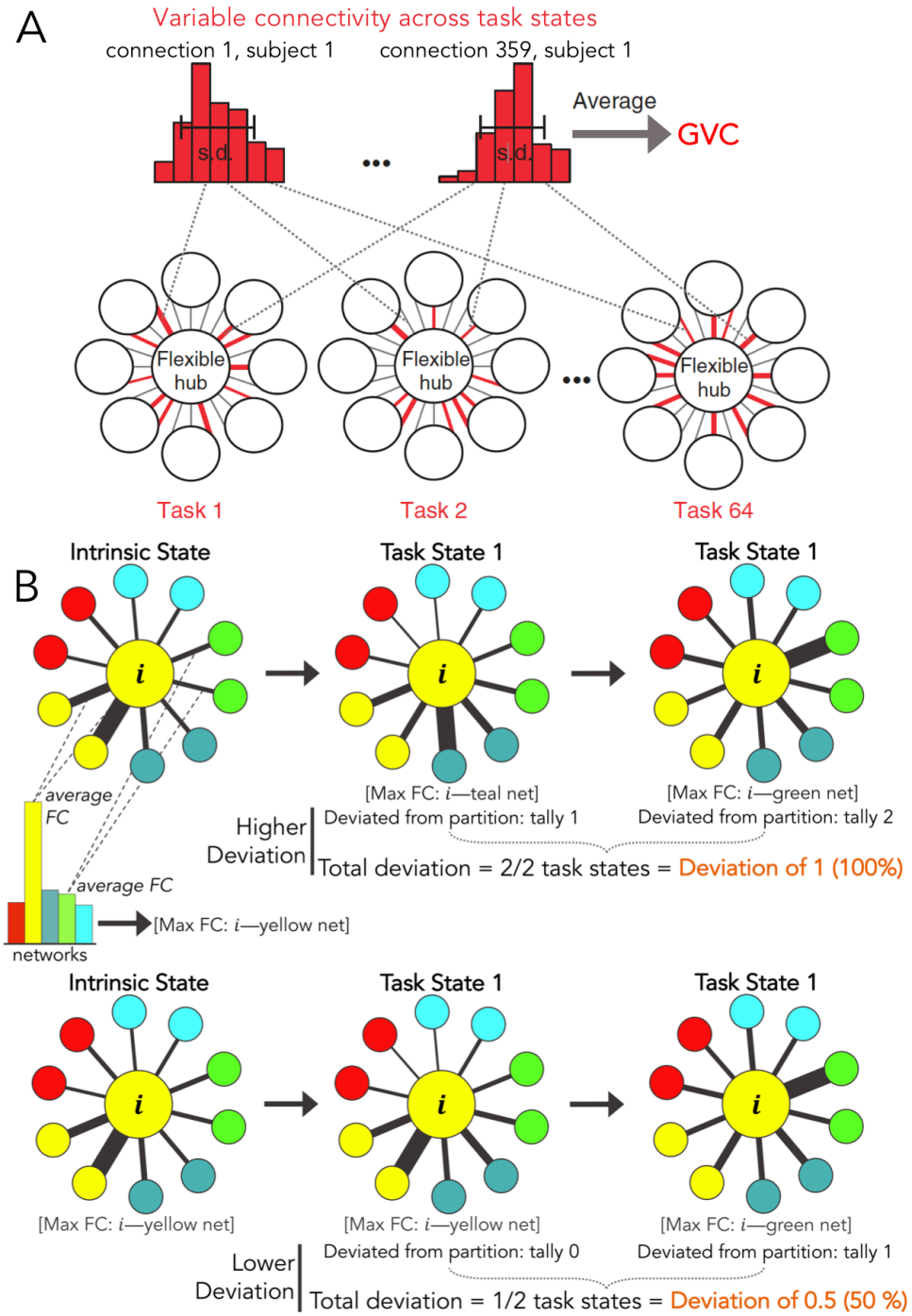

Figure 3. Schematic depictions of network metric algorithms. (***A***) Global variability coefficient (GVC), reproduced with permission (Cole et al., 2013b). Between-network variability coefficient (BVC) is measured equivalently, except within-network connections are withheld. (***B***) Network partition deviation. Per region (large yellow example node labeled "i"): each of its 359 connectivity estimates were averaged according to their empirically adjusted CAB-NP (see Materials and Methods) networks (bar graph in top example), resulting in 12 FC estimates per region. Network "preferences" (network location of maximum FC estimate; thickest lines) were tallied across task states. How often a given region deviated from its predefined partition (intrinsic state) was computed [tally / total number of tasks]. *Higher deviation*: the example region deviated in two out of two hypothetical states (100% deviation=deviation of

1). *Lower deviation*: the example region deviated in one out of two hypothetical task states (50% deviation=deviation of 0.5). The colored nodes encircling the example region represent example regions from example networks, and black lines of variable width represent FC estimates (edge weights).

Table 1. Graph theoretical diagnostic metrics for network reconfiguration properties across states.

Metric name	Formula	Measures; Diagnoses	Parameter-space?	Relies on a pre-defined partition?
Global Variability Coefficient (GVC)	$GVC_n = \frac{1}{N}\sum_{i=1}^{n}\sqrt{\frac{\sum_{l=1}^{T}(FC_{il} - \bar{x}_{FCl})^2}{T-1}}$	Variable FC across tasks; flexible hubs	No	No
Between-Network Variability Coefficient (BVC)	$BVC_n = \frac{1}{N'}\sum_{i'=1}^{n'}\sqrt{\frac{\sum_{l=1}^{T}(FC_{i'l} - \bar{x}_{FCl'})^2}{T-1}}$	Variable FC across tasks, between-network; flexible hubs	No	Yes
Network Partition Deviation (Deviation)	$Deviation_n = 1 - \left[\frac{\sum_{j=1}^{T}\left[\left(\max\left(\frac{\sum_{rS=1}^{c} FC_{cj}}{C}\right)\right) \in rS\right]}{T}\right]$	Network preference changes over time, compared to intrinsic partition; reassignment profile	Minimal	Yes

Table 1 summarizes the mathematical specifications of network metrics. Global variability coefficient (GVC; Cole et al., 2013b), between-network variability coefficient (BVC), and network partition deviation (novel) (named in ***column 1***) are described in terms of the following: (***Column 2***) their mathematical or algorithmic formulae. All equation symbols are expressed consistently. *Formula terms*: n=brain regions; T=tasks; i=region 1; l=task 1; N=number of regions; FC=weighted adjacency matrix; n'=out-of-network regions; i'=region 1, out-of-network; N'=number of out-of-network regions; $FC_{i'l}$=edge weight, per out-of-network region, per task; FCl'=FC matrix, out-of-network regions only, per task; j=last region; r=last task; γ=spatial resolution; ω=temporal resolution; P=optimization null-model; $Sij,_{l+1,r=}S$, all other tasks; c=network regions; C=number of network regions; rS=predefined partition; FC_{cj}=edge weight, per network-region, per task. (***Column 3***) What each metric measured and diagnosed. This was how results were interpreted, and mechanisms or properties were framed. (***Column 4***) If each metric relied on user-chosen parameters (e.g., had a parameter-space). (***Column 5***) If each metric relied on a predefined network partition (also see Materials and Methods).

Global Variability Coefficient (GVC)

GVC was originally developed by Cole et al. (2013b), and characterizes changing patterns of connectivity across task states by measuring the variability of interregional connectivity (Fig. 3A and Table 1). Thus, GVC treats spatial changes in connectivity, across states, as continuous. No parameters are required by the user and a predefined network partition is not necessary (aside from regional parcellation, as in the present study) (see Table 1).

In Cole et al. (2013b), FPN connections exhibited the highest GVC compared to all other networks. In that study, the FPN also maintained connectivity patterns that could decode task information (using an earlier version of the C-PRO paradigm). Further, FPN connectivity was found to vary systematically with similarity of C-PRO task states. Taken together this suggested that (1) FPN regions exert adaptive task control as flexible hubs, and (2) GVC results were not driven by noise. We replicated these findings and extended the analysis to CON connections. In brief, the 64 C-PRO task states have zero to two overlapping rules (Fig. 1). For example, one task's rules included *both, high pitch,* and *left middle*, and another included *both, red,* and *left middle*.

These example tasks had two overlapping rules (*both* and *left middle*). We created a 64 by 64 similarity matrix to quantify these overlap sets, and quantified the Spearman's Rho for FPN and CON connections for those sets. Next, we restricted the same analysis by only including FPN and CON regions with the highest GVC, in the following increments: top 10%, 8%, 6%, 4%, and 2%. This addresses whether highly variable connectivity (as measured by GVC) relates systematically to task context (Cole et al., 2013b).

Between-Network Variability Coefficient (BVC)

BVC was inspired by Cole et al. (2013b), and is related to between-network global connectivity in Ito et al. (2017). BVC is equivalent to GVC, except within-network connectivity estimates are withheld from the computation of standard deviation (Fig. 3A). This change from GVC accounts for the potential confound that within-network connections might confer upon results. In Cole et al. (2013b), FPN had the highest participation coefficient compared to all other networks, suggesting that FPN regions maintain many between-network connector hubs. BVC simply quantifies this in a manner closer to GVC. BVC (unlike GVC) required the use of a predefined network partition to define the regional bounds of each network. All other specifications of BVC are identical to GVC (see Table 1).

Network Flexibility (NF)

NF was originally developed by Bassett et al. (2011, 2013a, 2013b) to quantify how often (i.e., for how many tasks) a region changes its network "allegiance", and standardizes this by all possible changes. NF characterizes the spatiotemporal dynamics related to task-state time series by quantifying temporal variability in network partition solutions. These network partitions are determined by an optimized quality function for community detection termed multilayer modularity (also termed multislice or multiplex in some studies) (Louvain Q-modularity; Mucha et al., 2010). Thus, NF does not utilize a predefined network partition, but instead requires community detection to be applied per dataset. Required parameters (γ,ω) could be used to tune the degree to which connections were treated as discrete versus continuous in space (γ is the spatial resolution parameter) and/or time (ω is the temporal resolution, or coupling, parameter). In the present study, we swept a parameter space of γ and ω, ranged around their prototypical values (Bassett et al., 2013; Braun et al., 2015; Chen et al., 2015; Amelio and Tagarelli, 2017). We swept the modularity function's parameter space by ranging ω from zero to 2.0 in steps of 0.2; and γ from zero to 5.0 in steps of 0.5. For both free parameters, zero is the lower limit. An upper limit of 2.0 for ω was based on prior observations that task states tend to merge into one large state at higher coupling values (Bassett et al., 2013a). At the upper limit of γ (5.0), spatial resolution becomes acute and each region develops its own network. Additionally, the temporal dynamics conferred by ω are no longer available at the upper limit of γ (Chen et al., 2015; Amelio and Tagarelli, 2017). This sweep yielded an 11 by 11 matrix of NF estimates, per region (and per participant). We compared regional NF estimates to regional GVC estimates (both metrics were standardized, and Spearman's rank-order correlation quantified similarity in these measures across participants), to assess the point in the parameter-space wherein NF and GVC overlap most. These comparisons were performed for both the network-mean and regional-mean vectors.

Network Partition Deviation

Given that NF results varied by tuning parameter (see Results), we created a novel metric termed network partition deviation (or just "deviation"). The primary goal of developing deviation was to quantify network reconfiguration in a highly principled manner. This involved a principled definition for what it means for a region to "reconfigure": a change in the network community that a given region is most connected with (i.e., the network with the highest mean connectivity). Deviation was the percent of task states (more generally, the relative frequency across time), in which a given region's "preference" deviated from the predefined partition. To quantify this, deviation enumerated network reassignments from a predefined partition across task states (see Table 1 and Fig. 3B). Per task state and per region, connectivity estimates were searched for the maximum value. The network location of this maximum (relative to the predefined partition) was indexed as the network assignment preference for that given state. To illustrate how network reassignment was computed, we generated a video of the regional network preferences across task states, projected onto a standard brain schematic (see Multimedia 1). We used the Connectome Workbench software to generate these visualizations (Marcus et al., 2011).

We used the Cole-Anticevic brain-wide network partition (Ji et al., 2019), plus adjustments derived from the empirical resting-state fMRI data of the participants studied herein, as the predefined reference (see Materials and Methods section on network partitioning). This *a priori* network partition can be thought of as a minimal parameter space maintained by deviation in the present study, however future work may apply community detection (i.e., empirically-based network partition) if appropriate. Deviation may be accompanied by its complementary measure, network partition adherence, which was the relative frequency of states in which a given region *adhered* to its predefined network assignment (or 1-deviation, meaning that deviation and adherence add up to 1, or 100% of task states). We further unpacked deviation by depicting *which* networks were preferred by regions (when deviating from the partition), generating reassignment profiles.

Cognitive control cartographies

We rendered one primary mapping of cross-state network-reconfiguration properties, and two secondary mappings which broke up the primary mapping's properties into within-network and between-network scores. For the secondary mappings, within-network GVC was computed by setting between-network FC estimates to 'NaN' (i.e., 'not a number' in MATLAB) before inputting data into the GVC algorithm. Likewise, between-network GVC was computed by setting within-network FC estimates to 'NaN'. This effectively nullified the variability for those regions such that GVC ignored them during computation (which principally employs standard deviation across states; see Fig. 3A and Table 1). Between-network GVC was equivalent to BVC described above. Within-network deviation was computed by setting FC estimates of between-network regions to the resting-state FC for those regions before inputting data into the deviation algorithm. Likewise, for between-network deviation, we substituted within-network estimates with corresponding regions' resting-state FC. We considered the use of resting-state FC most appropriate given deviation's inherent comparison to the resting-state partition. Thus, deviation away from the resting-state partition would always be zero for regions set to their resting-state estimates. Extended Data Fig. 7-2 visually depicts the input data for each of these secondary cartographies.

Decoding Analyses

A minimum distance classification analysis (Haxby et al., 2001) was performed for each cognitive control network to test if control-network connectivity patterns could significantly decode task state. As in Cole et al. (2013b), three 4-way classifications were performed across FPN regions, as well as CON regions in the present study. Importantly, connectivity patterns were implemented as neural features in the present study given the focus on functional network interactions. Further, we extended the cohort to include N=50 (per discovery and replication datasets), used correlation as a classifying distance measure (Mur et al., 2009; Ito et al., 2017), and performed 8-fold cross validation. Classifiers were trained on a random subset (over 8 folds) of 56 task states and tested on the remaining 8 task states (64 altogether). The labels associated with these states were according to: (1) logic (both, not both, either, or neither), (2) motor (left middle, left index, right middle, or right index), and (3) sensory (vertical, red color, high pitch, constant tone) rule-set domains (see Fig. 1). Therefore, chance accuracy was 25% in each 4-way analysis. As in Ito et al. (2017), we averaged neural features across matching training-set labels (termed "prototypes", e.g., in the logic rule-set classification: training-set connectivity estimates that contained "both" were averaged). Within-subjects prediction accuracies were averaged across the 8 folds (Varoquaux et al., 2017).

We performed one-sample Anderson-Darling tests (AD-test) of normality on each cross-subject distribution of accuracy scores to assess whether parametric assumptions were met. In all cases, AD-test results were significant, indicating that accuracy scores came from a normal probability distribution. Thus, we performed one-sample, right-tailed student's t-tests against chance accuracy on the cross-subject prediction accuracy values. Further, a false discovery rate corrected $p<0.05$ threshold was applied across all hypothesis tests to control for family-wise error.

Code and Software Accessibility

We included all MATLAB, python, and demo code in a publically available platform. Data is available at the level of functional connectivity estimation, for the use of loading into demo scripts. Data at other levels of processing, or data otherwise presented in this study, are available upon request. The master GitHub repository for this study can be found here: https://github.com/ColeLab/controlCartography

Results

Intrinsic and Task-State Functional Connectivity

Replicating previous findings (Cole et al., 2014), cortex-wide rsFC (Fig. 4A) and tFC (Fig. 4B) estimates were highly similar. This significant similarity was observed for the average tFC taken across all 64 C-PRO tasks (Mantel-r=0.89, $p<0.00001$, R^2=0.79), as well as for each C-PRO rule individually (Extended Data Table 4-1). This aligns with previous observations that the set of networks present during rest are highly related to the set of networks present during task states. In addition to the minimal cognitive demands during rest providing a cognitive baseline for a variety of tasks, this result suggests that rest may be an appropriate reference state for characterizing changes in networks across multiple task states. The similarity observed between

rsFC and tFC (all 64 C-PRO tasks) in the replication dataset was comparable (Mantel-r=0.90, p<0.00001, R^2=0.81).

To summarize changing connectivity from the resting state to the average task state, we created a task versus rest difference matrix, and found 21% of those values to be significant differences (max-T critical threshold=5.46, 5,000 permutations). The finding that rsFC and tFC (across multiple task states) are highly correlated, yet the differences between them are nontrivial, justified subsequent analyses of functional reconfigurations between these two kinds of states. Findings were consistent in the replication dataset: approximately 32% significant rest-to-task differences (max-T critical=5.67).

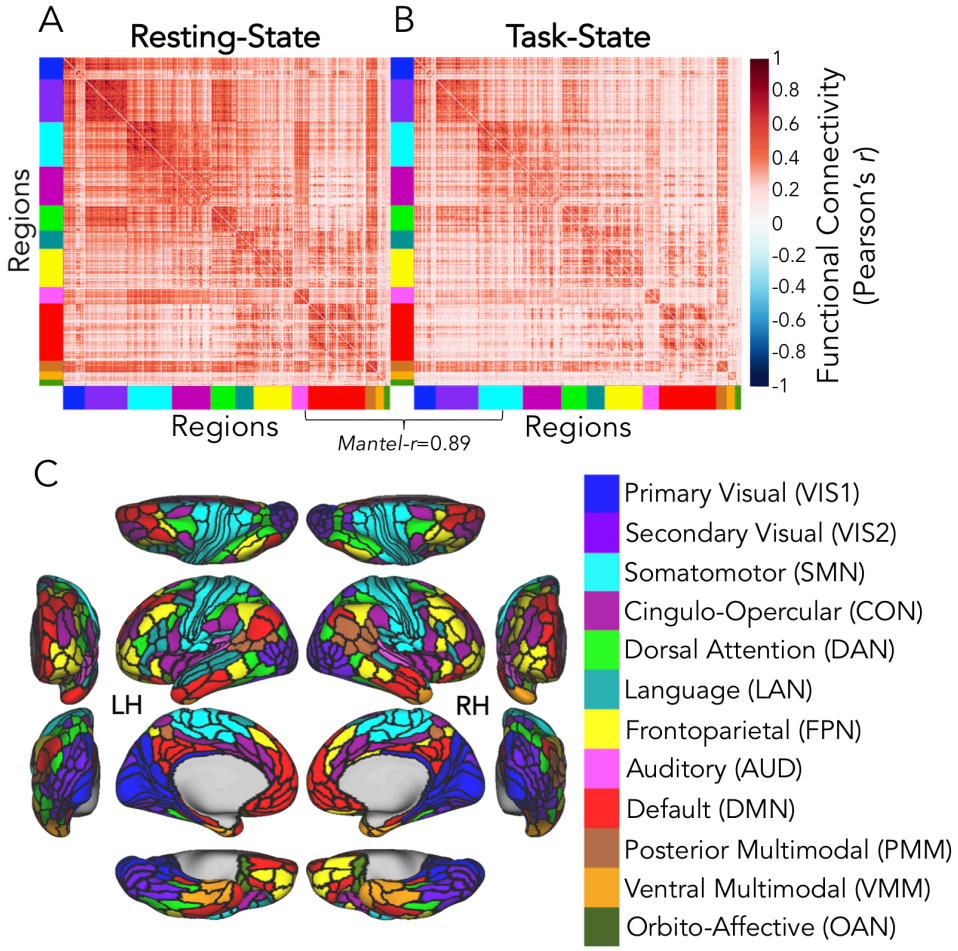

Figure 4. Functional connectivity (FC) estimation. (***A***) Resting-state functional connectivity (rsFC) across 360 by 360 regions (regional parcellation as in Glasser et al., 2016), ordered per the CAB-NP, adjusted by resting-state preferences (see Materials and Methods) (color-coded along each matrix edge as in C). Discovery-set grand averages are depicted. (***B***) Task-state functional connectivity (tFC) across 360 by 360 brain regions, ordered and estimated as in A (grand averages: n=50 and 64 C-PRO task states). (***C***) Cortical schematic of the Cole-Anticevic Brain-wide Network Partition (CAB-NP) (Ji et al., 2019), empirically adjusted by the resting-state preferences of the present participants (see Materials and Methods). LH = left hemisphere; RH = right hemisphere. Color-coding scheme of networks and acronyms listed in parentheses are used consistently throughout the present paper. Note that the two cognitive control networks of special interest included the CON (plum) and FPN (yellow).

Network Metrics: Variability Coefficients

Our prior work found that the FPN contains *flexible hub regions* – network nodes capable of rapid reconfiguration with changing task demands (flexible) that have extensive connectivity (hubs) (Cole et al., 2013b). Recent work has suggested that the CON also contains hub-like regions (Power et al., 2013; Ito et al., 2017), yet it is unknown if they are likewise flexible. Accordingly, we used two related metrics to assess if networks contain flexible hub regions (Cole et al., 2013b): global variability coefficient (GVC), and between-network variability coefficient (BVC) (see Materials and Methods, Fig. 3, and Table 1).

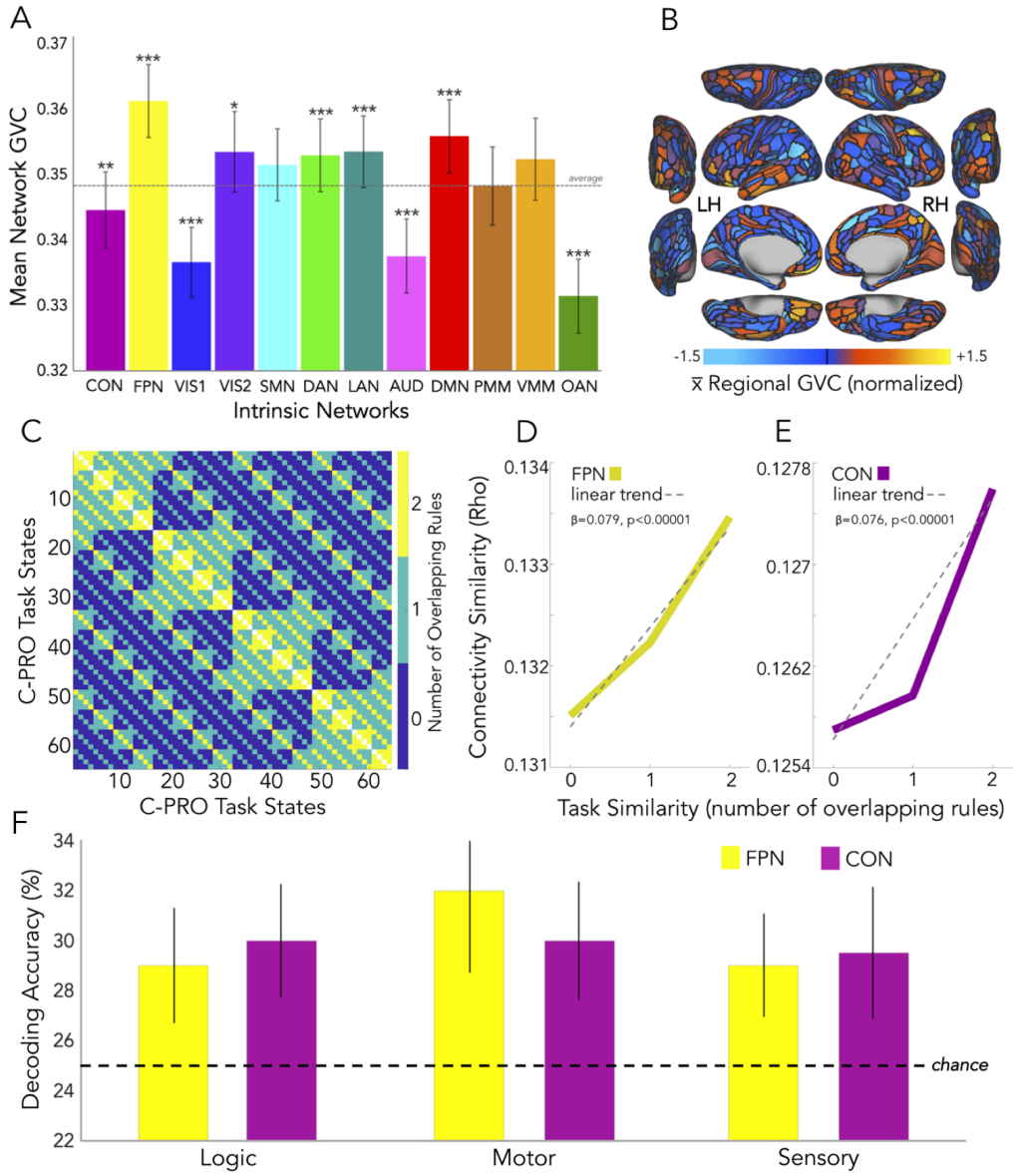

Figure 5. Global variability coefficient (GVC) and task representation. (***A***) Network-mean GVC, across n=50 and all C-PRO task states. Error bars: standard error of the mean. Asterisks: statistically significant t-tests, using the max-T approach (see Materials and Methods). Grey dashed line: mean GVC across networks. (***B***) Regional-mean GVC. (***C***) Similarity of C-PRO task states, represented by number of overlapping rules (0 overlapping rule=blue, 1 overlapping

rule=green, 2 overlapping rules=yellow). An overlap of 3 rules exists along the diagonal (white), but these connections were not included in analyses because connectivity similarity would be *Rho*=1 (identical task states). (*D*) Relationship between FPN connectivity similarity and task similarity. All connectivity estimates were included. Grey dashed line: linear trend, with associated beta and t-test significance listed. (***E***) Same as D, but for CON regions. The results in D and E demonstrated that control network connectivity similarity varied systematically with task similarity, suggesting that GVC results (A and B) were not driven by network noise. (***F***) Cross-subject (n=50, discovery dataset) mean decoding accuracies for logic, motor, and sensory rules (4-way classifications where chance accuracy was 25%). Black horizontal line: chance accuracy. Error bars: standard error of the mean. Both FPN and CON connectivity patterns significantly decoded task rules above chance, demonstrating their importance in task representation.

Critically, Cole et al. (2013b) only involved N=15 subjects, compared to the N=50 discovery and separate N=50 replication datasets in the present study. Thus, replicating the results of Cole et al. (2013b) would be nontrivial. Replicating the main result of Cole et al. (2013b), regions of the FPN had the highest GVC (Fig. 5A) and BVC (Extended Data Fig. 5-2A and 5-2B) compared to the mean of all other networks (GVC: max-$T(49)=10.94$, $p<0.0001$; BVC: max-$T(49)=10.69$, $p<0.0001$). BVC and GVC results were highly correlated at both the network (Fig. 5A) and regional levels (Fig. 5B) (network-wise: $r=0.9912$, $p<0.00001$, $R^2=0.9824$ cross-network shared variance; region-wise: $r=0.9972$, $p<0.0001$, $R^2=0.9944$ cross-region shared variance), suggesting that within-network estimates do not dominate the outcome of GVC analyses (see Extended Data Fig. 5-3A and 5-3B).

These results replicated in the replication dataset: the FPN demonstrated the highest GVC (Extended Data Fig. 5-1) and BVC (Extended Data Fig. 5-2C and 5-2D) compared to the mean of all other networks (GVC: max-$T(49)=7.23$, $p<0.0001$; BVC: max-$T(49)=6.93$, $p<0.0001$). GVC results highly overlapped between discovery and replication datasets (*Rho*=0.9091, $p<0.00001$). BVC and GVC results were also tightly correlated at both the network and regional levels in the replication dataset (network-wise: $r=0.9925$, $p<0.00001$, $R^2=0.985$ cross-network shared variance; region-wise: $r=0.9975$, $p<0.0001$, $R^2=0.995$ cross-region shared variance) (Extended Data Fig. 5-3C and 5-3D). Additionally, both GVC and BVC results highly overlapped between discovery and replication datasets (GVC: *Rho*=0.9091, $p<0.00001$; BVC: *Rho*=0.881, $p=0.0002$) (Extended Data Fig. 5-1 and 5-2).

In conjunction with many studies reporting increased FPN activity as a function of cognitive control demands (Yeo et al., 2015), this pattern of results supports the notion that the FPN contains flexible regions adaptively configured for multitask control. Further, we compared GVC between control networks and each of the other networks. FPN regions were significantly higher than each other network (using the max-T approach, $p<0.0001$), except for the ventral multimodal network. CON regions were significantly different (typically lower) than each other network on the measure of GVC (using the max-T approach, $p<0.0001$), except for posterior multimodal and ventral multimodal networks. Lastly, a paired-samples t-test comparing FPN and CON revealed a significant difference in GVC scores ($t(49)=11.68$, $p<0.00001$), suggesting that the two proposed control networks exhibit distinct variability of global connectivity. In the replication dataset, FPN regions' GVC scores were also significantly higher than each other network, except for the ventral multimodal network (orange bar in Extended Data Fig. 5-1). CON regions were significantly different than each other network on the measure of GVC in the replication dataset, with no exceptions (Extended Data Fig. 5-1). The paired-samples t-test contrasting FPN and CON

specifically also showed a significant difference on GVC scores in the replication dataset ($t(49)=10.55$, $p<0.00001$).

Despite evidence that FPN has strong global variability consistent with flexible hubs, it remains unclear if that variability is systematically related to task information content – a prerequisite for flexible hubs to implement task-related reconfigurations. Prior findings (Cole et al., 2013b) demonstrated that FPN connections systematically vary with increasing task-state similarity. We sought to replicate this result in FPN and – given the current focus on cognitive control systems – we additionally analyzed CON connections. As in Cole et al. 2013b, task-state similarity was taken as the number of overlapping, or shared, rules presented to participants, across all 64 tasks (Fig. 5C; also see Materials and Methods). We then measured Spearman rank correlations (as a score of similarity) amongst connections according to these task-state pairings, for both FPN (Fig. 5D) and CON regions (Fig. 5E). An approximately linear relationship was observed, suggesting that shifts in connectivity systematically relate to shifts in task state, and are not simply a byproduct of noise. Note that at the subject level, the effect size of shifting connectivity is not interpretable because it is unknown how many connection changes are required to cognitively implement a task-rule change (e.g., two robust connection changes may be enough cognitively, but produce small correlation changes at the network level). The linear regression weights of these similarity scores were consistently different from zero across subjects (FPN: $t(49)=35.51$, $p<0.00001$; CON: $t(49)=33.25$, $p<0.00001$). Next, we performed the same analyses, but restricted the connections to those maintaining the highest variability (across top 2% to 10% in steps of 2%) across task states (i.e., the "VC" of GVC) for both the FPN (as in Cole et al., 2013b) and CON. Results were similar to the main results across all thresholds, with linear weights significantly different from zero ($p<0.05$). These results suggest that GVC results are likewise driven by systematic changes in connectivity, and not network noise. These results additionally reveal that CON also systematically changes its global connectivity pattern according to task goals, though the GVC results suggest these systematic changes are smaller in CON (and most other networks) than FPN.

Next, we tested the hypothesis that global FPN and CON connectivity patterns were specific enough to each task set that they could be used to reliably predict the current task rules being used. As in Cole et al. (2013b), FPN (as well as CON in the present study) features were restricted by their somatomotor network (SMN) connections in the tests of motor-domain rule classification. Firstly, we tested how well control network connectivity patterns could decode rule sets in the three C-PRO domains (logic, sensory, and motor; see Fig. 1). In each domain there were four distinct rules, thus chance accuracy was 25% (see Materials and Methods). FPN whole-cortex connectivity patterns could be used to significantly decode rule sets in logic and sensory domains (logic: $t(49)=1.74$, $p=0.044$; sensory: $t(49)=1.94$, $p=0.029$) and FPN to somatomotor connectivity patterns could be used to significantly decode motor domain rules ($t(49)=2.14$, $p=0.019$) (Fig. 5F, yellow bars). Likewise, CON whole-cortex connectivity patterns could be used to significantly decode rule sets in logic and sensory domains (logic: $t(49)=2.21$, $p=0.016$; sensory: $t(49)=1.70$, $p=0.047$) and CON to somatomotor connectivity patterns could be used to significantly decode motor domain rules ($t(49)=2.11$, $p=0.019$) (Fig. 5F, plum bars). Statistically significant decoding results were also observed in replication dataset participants (FPN logic: $t(49)=1.94$, $p=0.029$; FPN sensory: $t(49)=2.14$, $p=0.019$; FPN motor: $t(49)=1.77$, $p=0.042$; CON logic: $t(49)=2.47$, $p=0.009$; CON sensory: $t(49)=2.40$, $p=0.01$; CON motor: $t(49)=2.45$, $p=0.009$). All

t-tests results passed an FDR-corrected $p<0.05$ threshold (see Materials and Methods). The capacity for control networks' global connectivity patterns to significantly decode task rules in all three domains suggests that each of their network interactions carry information critical to task representation.

Network Metric: Flexibility

Network Flexibility (NF) measures functional network dynamics related to task-state time series (Mucha et al., 2010; Bassett et al., 2011, 2013a, 2013b; Cole et al., 2014), and is thus highly relevant to our current hypotheses regarding control network reconfigurations. Conceptually, NF is aligned with GVC, particularly as both quantify large-scale changes in functional network configurations. However, it is unknown whether these metrics capture the same aspects of network reconfiguration. The computations of both GVC and NF are oriented around a measure of network change, however, the approaches are distinct enough to hypothesize that NF and GVC will not entirely overlap. We hypothesized that differentiation between NF and GVC would lend insight into the nature of control network reconfiguration. In particular, GVC assesses continuous changes in connectivity strengths, while NF assesses discrete network reassignments.

The multilayer modularity step required parameters ω (temporal resolution or "coupling") and γ (spatial resolution) to be chosen. The standard values used for these parameters across multiple studies are γ=1 and ω=1 (Bassett et al., 2013b; Chen et al., 2015; Braun et al., 2015). NF that resulted from community detection at γ=1 and ω=1 was termed NF-standard (Extended Data Fig. 5-4). Since there is only limited theoretical basis for those parameter choices we computed NF across a range of values around these standards, such that γ was varied between zero and five in steps of 0.5; and ω was varied between zero and two in steps of 0.2 (see Materials and Methods). These sweeps resulted in 121 vectors of regional NF estimates (per participant). It was clear that results depended substantially on the exact values of γ and ω, such that we were unable to make systematic inferences regarding flexibility of network assignments using NF. To illustrate this: we identified parameters (γ=2.5 and ω=0.2) that yielded high cross-node similarity to GVC, termed NF-matched (discovery dataset: *Rho*=0.8169, $p<0.00001$; replication dataset: *Rho*=0.6993, $p=0.015$) and others γ=0.5 and ω=0.2 that yielded a negative relationship with GVC, termed NF-unmatched (discovery dataset: *Rho*=-0.4546, $p=0.14$; replication dataset: *Rho*=-0.3077, $p=0.34$), while the NF-standard parameters (γ=1 and ω=1) yielded a positive but not significant relationship with GVC (*Rho*=0.4825, $p=0.12$; replication dataset: *Rho*=0.3147, $p=0.32$) (Extended Data Fig. 5-4 and 5-5).

Network Metric: Partition Deviation

Given that NF demonstrated inconsistent results dependent on tuning parameters, we created a novel metric, Network Partition Deviation (or simply, deviation), that could quantify network reconfiguration without the need for a parameter search. Deviation enumerates network reassignments across task states by quantifying the percent of states (i.e., the relative frequency across tasks) in which a given region deviates from a predefined partition (see Materials and Methods, Fig. 3B, Table 1, and Multimedia 1). We employed the CAB-NP adjusted by the empirical resting-state data of participants herein (Fig. 4C and Extended Data Fig. 4-1) as the intrinsic, predefined reference (see Materials and Methods). See prior work (Cole et al., 2014; Krienen et

al., 2014) and the results section "Intrinsic and Task-State Connectivity" above for evidence that the resting state provides an appropriate intrinsic network configuration to act as a reference for assessing network deviations.

Of the cognitive control networks of interest here – the CON and the FPN – the CON displayed the highest mean deviation, which was significantly higher than the mean across all other networks (max-$T(49)=12.74$, $p<0.0001$) (Fig. 6A). Moreover, the FPN demonstrated deviation that was near the mean, and was not significantly different from the mean across all other networks. This contrasted from the conclusions drawn from GVC, which showed the FPN significantly above the mean, and the CON significantly below it. Similarly in the replication dataset, CON regions' deviation scores were again significantly higher than the mean of all other networks (max-$T(49)=16.33$, $p<0.0001$) (Extended Data Fig. 6-1A).

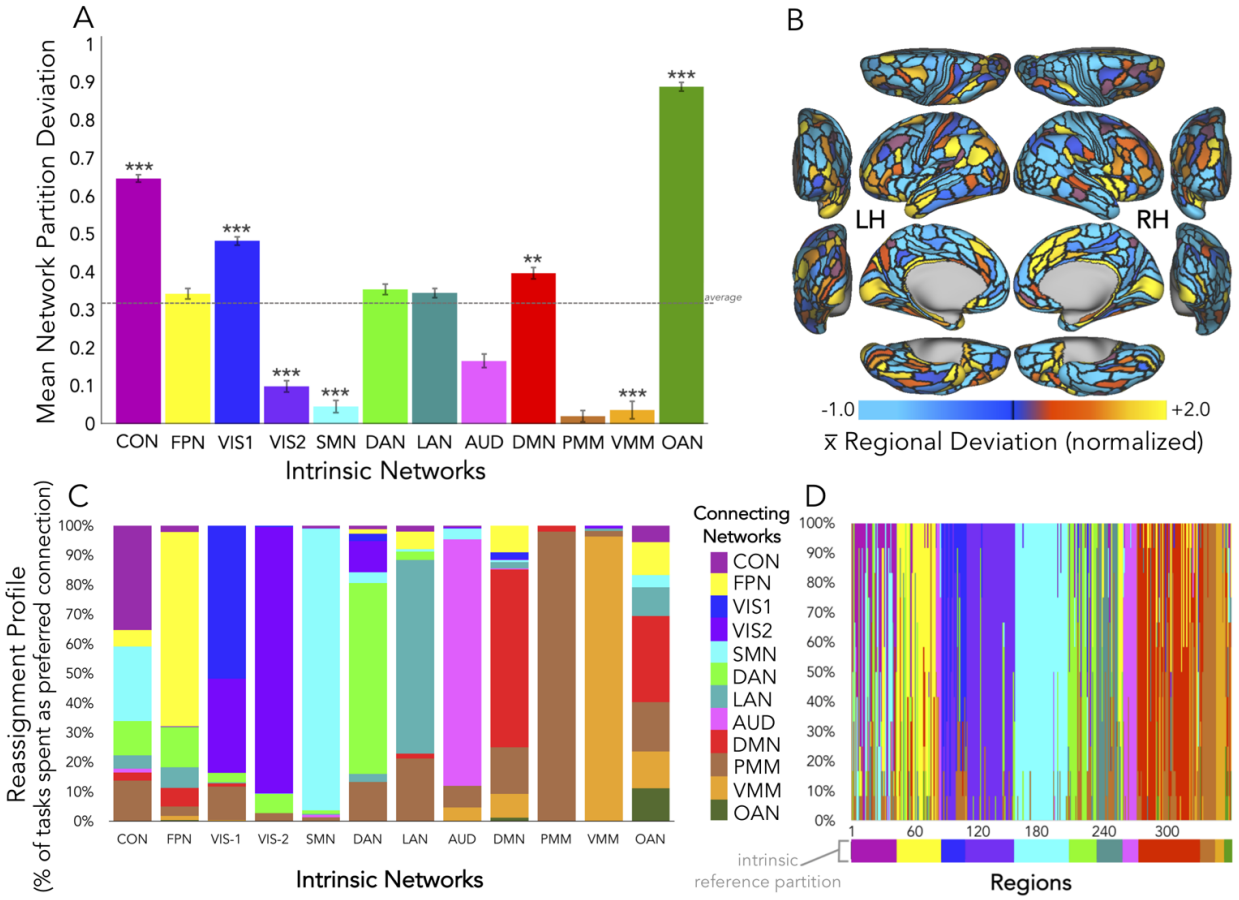

Figure 6. Network Partition Deviation. Mean, error bars, and hypothesis testing specifications were the same as in Figs. 5, where asterisks mark statistically significant t-tests, using the max-T approach (see Materials and Methods; 10,000 permutations). (***A***) Network-mean deviation. See Discussion section for interpretations of the orbito-affective network (OAN). (***B***) Regional-mean deviation. (***C***) Network-level reassignment profiles. For each intrinsic network (x-axis), adherence (or 1-deviation) is depicted as the portion of the bar (connecting network) with the equivalent color. All other colors codify exactly which connecting networks were being preferred (see Table 1 and Methods for computation of deviation) when deviating from the predefined partition. That is to say, deviation in (A) is expanded in (C) to show frequency of reassignments, across task states (i.e., affinities). (***D***) The same as in (C), but the x-axis is depicted at the regional level (i.e., these regional reassignments were averaged to generate C).

Next, we performed planned contrasts of the control networks' deviation scores versus each other networks' deviation scores, using the max-T method to correct for multiple comparisons (see Materials and Methods). The CON's deviation was significantly higher than every other network (p<0.0001), except for the orbito-affective network. Deviation estimates of FPN regions were significantly different from about half of the other networks (p<0.0001), including: secondary visual, somatomotor, cingulo-opercular, auditory, posterior multimodal, ventral multimodal, and orbito-affective. The deviation of FPN and CON regions were significantly different (t(49)=6.28, p<0.00001), suggesting that the control networks differ on how often they deviate from their intrinsic partitions across task states. In the replication dataset, CON regions' deviations scores were significantly higher than each other network, except for the orbito-affective network (Extended Data Fig. 6-1). Lastly, the paired samples t-test to compare the deviation of CON and FPN in the replication dataset likewise showed a significant difference (t(49)=9.13, p<0.00001).

To further explore the task-state reconfiguration property that deviation was capturing, we generated "reassignment profiles" at both the network (Fig. 6C) and region (Fig. 6D) levels. Reassignment profiles showed precisely which networks were preferred when a region was deviating from the intrinsic partition. As shown in Fig. 6C, the CON deviated to many other networks in an evenly-distributed manner (relative to other networks' reconfigurations) with some bias to somatomotor connections, whereas the FPN deviated less overall and with more specific preferences, favoring the dorsal attention, language, and default networks (in addition to itself). These reconfiguration preferences were consistent in the replication dataset profiles, as seen in Extended Data Figures 6-1C and 6-1D. As with other graph metric results, deviation estimates highly overlapped between discovery and replication datasets (*Rho*=0.958, p<0.00001), as did reassignment profiles (*Rho*=0.848, p<0.0001) (Extended Data Fig. 6-1).

Network Cartographies

We found that FPN regions expressed high GVC yet relatively low deviation. In contrast, CON regions displayed lower GVC yet higher deviation. Altogether, the CON and the FPN both exhibited higher reconfiguration properties than other networks. However, the diversity of findings across network metrics suggested that composite, multidimensional profiles were warranted to fully map out their functionalities. Careful examination of network metric estimates for CON and FPN regions clarified the pattern of results. FPN connectivity tended not to deviate (and when it did, to only a small number of networks as in Fig. 6C and 6D), whereas CON connectivity was more uniform (or "evenly" deviating, as in Fig 6C and 6D). Figure 7A depicts prominent network properties in a cartographic manner (Guimerà and Nunes Amaral, 2005; Mattar et al., 2015), charting GVC on the y-axis against deviation on the x-axis. The FPN can be found in the upper right quadrant of this cartography, near the mean demarcation line for deviation (the vertical gray line, Fig. 7A), pointing to the high-variability yet low-deviation performance of FPN regions in response to cognitive control task state changes. The CON can be found in the lower right quadrant of the cartography in Fig. 7A, suggesting a low-variability yet high-deviation complement to FPN in properties supporting cognitive control.

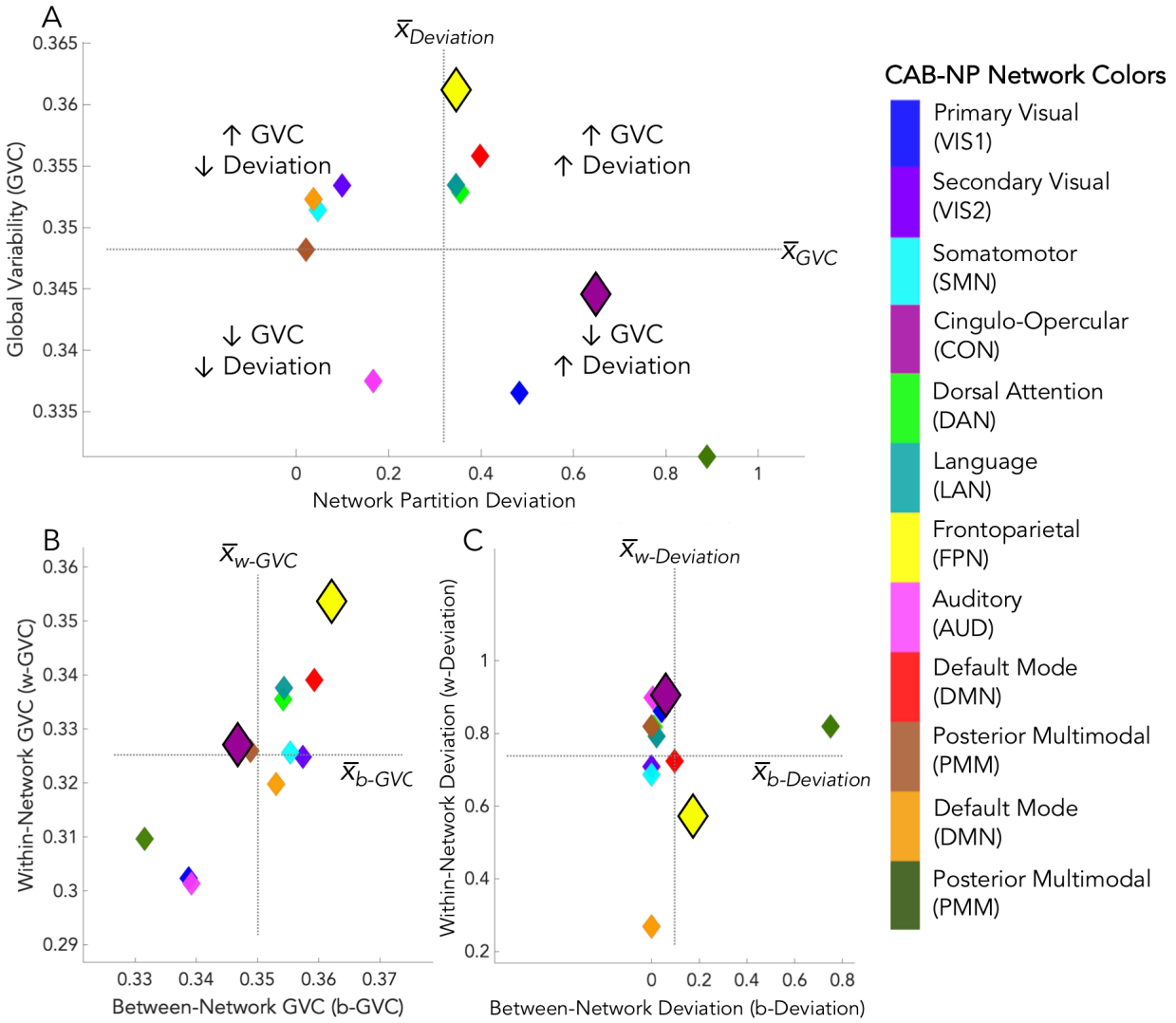

Figure 7. Cognitive control cartographies. (***A***) GVC (as in Fig. 5A) plotted over deviation (as in Fig. 6A), with demarcation lines (dashed and crossed gray lines) indicating the cross-network mean for each dimension (all axes are centered at these marks for ease of viewing). This allowed us to "map out" multidimensional properties at once. For example, networks in the lower right quadrant of A (such as CON) exhibit GVC lower than the mean and deviation higher than the mean. This mapping suggests a nonlinear relationship between GVC and deviation, suggesting that each measure characterizes a unique network property. In all panels, control network diamonds (FPN: yellow, CON: plum) are highlighted with dark black outlines and are larger than other network diamonds, with the sole visualization purpose of standing out as cognitive control networks. (**B**) GVC scores (y-axis of panel A) expanded by within-network and between-network values. (**C**) Deviation (x-axis of panel A) scores expanded by within-network and between-network values. The far-right legend depicts the CAB-NP color scheme (as in Fig. 4C) used for the diamonds.

To expand upon the primary mapping in Fig. 7A, we generated two secondary cartographies that depict the quantification of each primary measure's within-network and between-network scores (see Materials and Methods). Briefly, within-network dynamics were assessed by keeping the between-network connectivity fixed across states (defined by resting state). Similarly, between-network dynamics were assessed by keeping the within-network

connectivity fixed across states (defined by resting state) (see Extended Data Fig. 7-2 for data input schematics). Figure 7B charts these dimensions of GVC, showing both within-network and between-network FPN connections to be high on global variability, and CON to be near-mean on both within-network GVC and between-network GVC. Figure 7C depicts within- and between-network deviation. Both FPN and CON regions were near the mean for between-network deviation (yet on opposing sides of the mean, see vertical gray line in Fig. 7C), yet low and high, respectively, for within-network deviation. This suggests that CON's high deviation was driven primarily by changes in within-network connectivity.

Supporting dissociation of FPN and CON in terms of network dynamics, we directly compared FPN and CON regions on each secondary cartographic metric (Fig. 7B and 7C), and found the following: (1) FPN was significantly higher than CON on within-network GVC ($t(49)=8.92$, $p<0.00001$); (2) FPN was significantly higher than CON on between-network GVC ($t(49)=11.43$, $p<0.00001$); (3) CON was significantly higher than FPN on within-network deviation ($t(49)=6.55$, $p<0.00001$); and (4) FPN was significantly higher than CON on between-network deviation ($t(49)=4.88$, $p=0.000012$) (see prior results sections for FPN versus CON comparisons on GVC and deviation scores related to Fig. 7A, where all regions were included). This pattern of results replicated in the replication dataset: 1) FPN was significantly higher than CON on within-network GVC ($t(49)=8.65$, $p<0.00001$); (2) FPN was significantly higher than CON on between-network GVC ($t(49)=10.26$, $p<0.00001$); (3) CON was significantly higher than FPN on within-network deviation ($t(49)=6.16$, $p<0.00001$); and (4) FPN was significantly higher than CON on between-network deviation ($t(49)=2.13$, $p=0.03$) (Extended Data Fig. 7-1C and 7-1D).

To explore these results further, we created a color-coded graph of the partition reassignments captured by each version of deviation (Fig. 8). To quantify the relationships between reassignment patterns we used the Jaccard similarity index (see Materials and Methods). We found FPN's between-network deviation (i.e., within-network connectivity held constant) was more similar to "all-data" deviation than its within-network deviation (i.e., between-network connectivity held constant): Jaccard indices of 0.29 and 0.18, respectively. Yet, CON's within-network deviation was more similar to "all-data" deviation than its between-network deviation (Jaccard indices of 0.31 and 0.16, respectively). Supporting dissociation of FPN and CON network dynamics, the Jaccard similarity indices for CON and FPN were significantly different (Jaccard for deviation all-data and deviation within-network data, CON vs FPN: $t(49)=3.30$, $p=0.0018$; Jaccard for deviation all-data and deviation between-network data, CON vs FPN: $t(49)=-4.61$, $p=0.00003$).

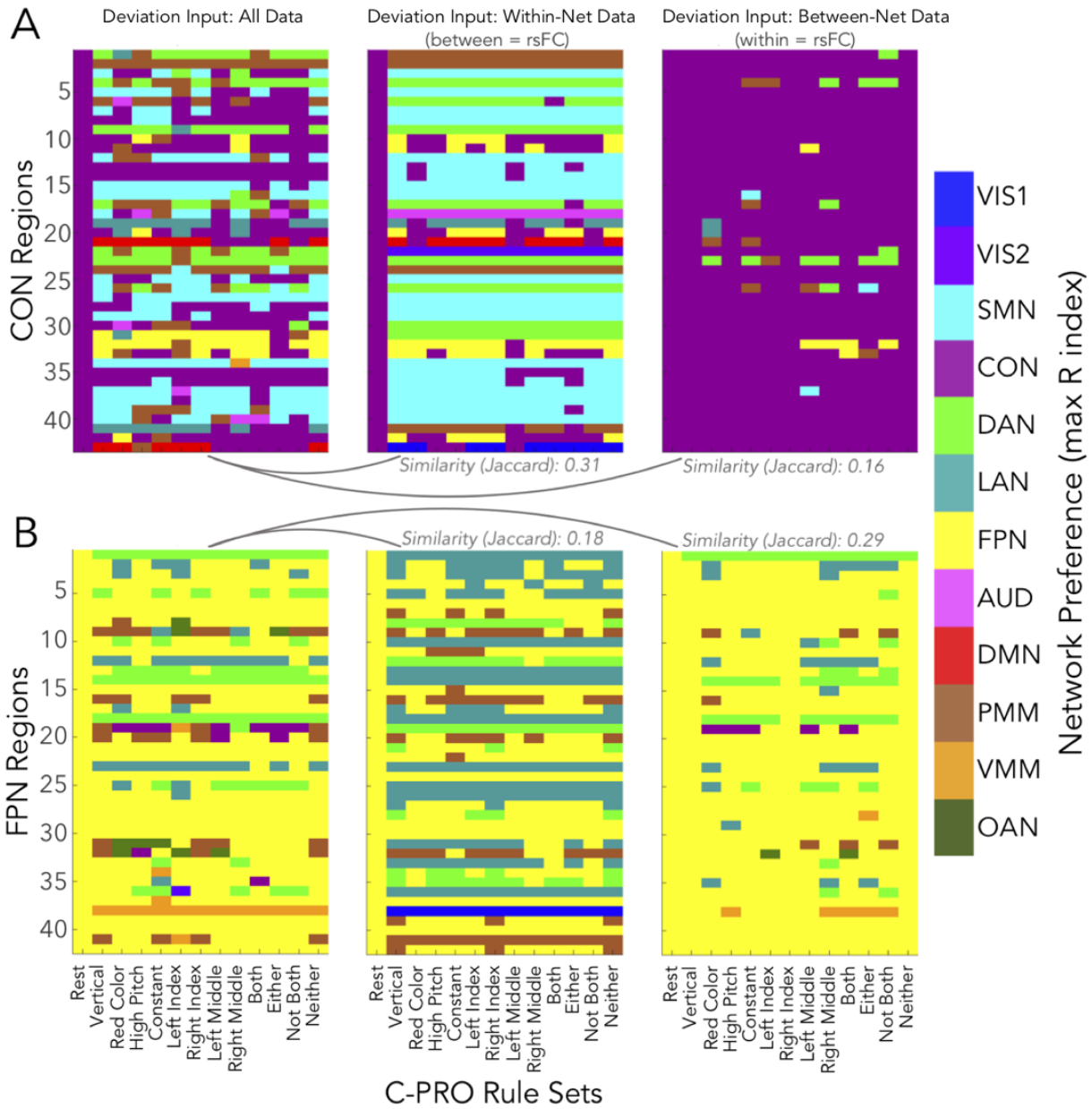

Figure 8. Reassignments conferred by the variants of network partition deviation in the control cartographies. Reassignment is the network index (based on the intrinsic partition) of the highest mean connectivity estimate (see Materials and Methods), per task state. In each panel, Jaccard indices are listed to indicate similarity between two partitions. Network assignments are color coded (as in Fig. 4C), and the 64 C-PRO task states are collapsed into 12 rule sets (plus Rest as a reference on each x-axis). (***A***) *Left*: Network reassignments of CON regions from the deviation algorithm, with all connectivity data included in the input (Fig. 7A, x-axis). *Middle*: Within-network CON estimates used in the deviation algorithm (Fig. 7C, y-axis). The Jaccard similarity of within-network and all-data deviation is 0.31. *Right*: Between-network CON estimates used in the deviation algorithm (Fig. 7C, x-axis). The Jaccard similarity of between-network and all-data deviation is 0.16, which is lower than the within-network similarity to all-data. (***B***) Same as panel A, except for FPN regions. The Jaccard similarity scores are: within-to-all=0.18, between-to-all=0.29. Thus, FPN showed the reverse pattern to CON, where between-network deviation is more similar to all-data deviation than within-network deviation.

This result supports the conclusion that the high deviation exhibited by the CON was driven by its within-network connections, indicating that CON task-related dynamics were driven mostly by reduction in within-network intrinsic connectivity (network "disbanding") to increase the strength of between-network connections relative to (now-reduced) within-network connections. In contrast, FPN regions maintained their within-network connection patterns while varying their between-network connection patterns across rest and task. This is consistent with FPN maintaining its intrinsic within-network connectivity while reconfiguring its between-network connections in a task-specific manner. Moreover, the pattern of CON within-network decreases were task-specific (Fig. 5E-5F and Fig. 8) This is consistent with CON being a flexible hub network like FPN, but with a distinct mechanism involving "switching" from within-network to out-of-network connectivity via dynamic reduction of within-CON connectivity.

Discussion

The chief conclusion of the current study was that combining network science measures into network cartographies (multi-dimensional functional "mappings") allowed us to characterize cognitive control brain systems acting as either flexible coordinators (frontoparietal regions) or flexible switchers (cingulo-opercular regions). The cartographies consisted of two primary dimensions: 1) GVC, measuring global FC reconfiguration across task states in a continuous manner and, 2) deviation, measuring global FC reconfiguration from rest to task in a discrete manner (Fig. 7). We found that FPN exhibited high GVC but low deviation, while CON showed the opposite pattern, consistent with complementary mechanisms of cognitive control. FPN appeared to act as a "flexible coordinator", based on its extensive between-network FC reconfiguration along with maintenance of within-network FPN connections across rest and task states. In contrast, CON appeared to act as a "flexible switcher", based on CON regions extensively reducing their within-network connections from rest to task to effectively switch to other networks during tasks (Fig. 2).

The present findings are broadly consistent with the view proposed by Dosenbach et al. (2006, 2007, 2008), which posited – based on fMRI task activations and resting-state FC – that control networks implement dissociable mechanisms. That work demonstrated FPN regions enacting control in a manner described as "active, adaptive, and online". We used tFC along with dynamic graph-theoretic measures to expand upon this, and observed high tFC-based global variability. This is consistent with adaptive monitoring and adjustment important for controlled processing (Cole and Schneider, 2007; Sadaghiani and D'Esposito, 2015; Crittenden et al., 2016). In contrast to FPN, Dosenbach et al. (2006, 2007, 2008) proposed that CON underlies "stable set maintenance, task mode, and strategy" (also shown by Vaden et al., 2013). While we did find CON connectivity changes to be more consistent (across task states) than FPN (Fig. 5A), we propose that its functional switching relates to the biased competition model and related theories.

The biased competition model posits that neural representations compete for resources, such that stimuli, actions, and/or thoughts compete for attention during task performance (Desimone and Duncan, 1995). The theory suggests that competition is biased by top-down goal-related signals from prefrontal cortex and related areas (i.e., control networks). These top-down control signals are thought to shift the competition in bottom-up processing (e.g., in visual

cortex), such that goal-relevant processes become more salient and more likely to "win". For instance, a top-down control signal could bias color-naming representations over word-reading representations to aid in Stroop task performance. This theory was built upon by the guided activation theory (Miller and Cohen, 2001) and flexible hub theory (Cole et al., 2013b). In line with these later theories, we recently posited that such top-down biases to bottom-up competitive processes are especially important for RITL paradigms (such as the C-PRO task), and that they are implemented by tFC changes from control networks (Cole et al., 2017). In the present study, connectivity patterns of FPN and CON regions significantly decoded C-PRO task rules (Fig. 5F). This suggests that distributed interactions implemented by the cognitive control networks critically support task representations. Further, network science measures probing those interactions suggested that top-down biases are implemented via two complementary mechanisms. First, CON regions appear to flexibly switch to other networks in a task-dependent manner, likely lending more "weight" or "energy" to help task-relevant regions/networks win competitions with other regions/networks. In support of this, we observed CON regions switching to other networks with a relatively uniform distribution (across tasks and switched-to networks) (Fig. 5 and Fig. 6C), and with high deviation across tasks (Fig. 6A), suggesting that CON was transiently disbanding and switching networks to lend resources to other goal-relevant networks. Second, FPN regions appeared to flexibly coordinate their global patterns of goal-driven biases by maintaining within-network connectivity. This likely facilitates the coordination of complex task sets via combinations of task rule representations. This account illustrates a fundamental trade-off in controlled processing: lending of resources by CON to help goal-relevant brain systems win competitions (e.g., with distracting stimuli), versus implementing goal-relevant "programs" by FPN through coordinated top-down biases.

Interestingly, FPN's between-network connectivity patterns were variable, but FPN's within-network intrinsic configuration remained intact across task states (Fig. 2 and 8). On the one hand, between-network FC variability corroborates the notion that FPN regions support task-specific coding (Crittenden et al., 2016) and selective attention demands (Sadaghiani and D'Esposito, 2015). On the other hand, within-network FC preservation suggests that FPN regions are *coordinating* the FC changes across FPN regions. These dynamics are well-suited to address the "variable binding" problem (Feldman, 2013), where variable stimulus information must be linked to task rules to enact cognitive computations. For example, in C-PRO tasks, variable rules must link via logical operations to perform a given task, and variable stimuli must link to those rules to produce correct behavior (Fig. 1). The maintenance of FPN's intrinsic organization combined with between-network reconfigurations, suggests a coding process that includes FPN, along with other, task-specific regions. This computational format would allow for variable stimulus information to be bound on a task-to-task basis. We propose that FPN's role in this scheme is to flexibly coordinate task-specific coding. Notably, this would impose high processing demands on FPN regions, which we suggest to be facilitated by the CON freeing up resources, pointing to a computational trade-off across these two cognitive control networks.

Two other networks joined CON in having low variability and high deviation: the OAN and the primary visual network (VIS1). OAN had both the lowest GVC and the highest deviation of all networks. This suggests that the switching mechanism proposed for CON also occurs for OAN, though other studies suggest distinct functionality for OAN. OAN is localized to a small number of regions in a single anatomical cortical location – ventromedial prefrontal cortex (and nearby

subcortical regions) (Ji et al., 2019). Human lesion studies and animal models suggest a core role of OAN in emotion processing and value representation (Roy et al., 2012), and likely receives direct dopaminergic projects from the ventral tegmental area (Seamans and Yang, 2004). Emotion processing may seem counter to the non-emotional C-PRO paradigm, yet evidence from human lesion studies (Koenigs et al., 2007) and neuroimaging (Botvinick and Braver, 2015) demonstrates that emotion, in the form of motivation, biases competition between outcomes during complex decisions. Future research should assess whether OAN provides a similar mechanism to CON for top-down biasing of cognitive processing, but via an emotional/motivational mode of processing. In contrast to OAN and CON, VIS1 was not diverse in its connectivity switches, primarily switching to the secondary visual network (extrastriate cortex) (Fig. 6C and D), consistent with integrated visual processing across the two visual networks.

Aside from the high-variability/low-deviation and low-variability/high-deviation cartographic mappings of the FPN and CON, respectively (Fig. 7A), there were two other scenarios possible. First, high-variability and high-deviation across task states, indicating fluctuating connectivity as well as notable partition reassignment from rest to task. The default mode network (red diamond in Fig. 7A) was the only network trending in this direction. Secondly, low-variability and low-deviation across task states, indicating stable connectivity estimates and adherence to the intrinsic partition from rest to task. The auditory network was the only observed herein (pink diamond in Fig. 7A), which may relate to sensory regions being proposed to have a "rigid core" organization (Bassett et al., 2013b). Other sensory-motor networks exhibited especially low deviation (compared to cognitive networks), suggesting low vs. high deviation was indicative of sensory-motor vs. cognitive network properties. Future work is warranted to explore this further, particularly if diverse task paradigms are implemented.

An essential consideration for future studies regards the question of timescale. Dosenbach et al. (2007, 2008) found increases in CON activity to be sustained across tasks, while FPN activations were present at task onset, then adaptively varied with changing task demands. In the present work, we applied network metrics across a set of dynamic task states demanding high levels of cognitive control. While measures of global variability summarized varying connectivity patterns across states, further examination is required to better determine the timescales of control network mechanisms. Relatedly, future work should consider how electrophysiological signatures of neural processing and network properties relate in terms of the instantiation of cognitive control. In resting-state based studies, Sadaghiani et al. (2010, 2012) found distinctions between FPN and CON based on alpha band signatures. Spontaneous activity in CON related to increases in global power, while FPN activity related to increases in long-range phase synchrony, corresponding to the functions of tonic alertness and phasic control, respectively. In future work, both rest and task states (cognitive control paradigms) should be assessed via alpha band signatures, as well as potential changes in those signatures from rest to task. A potential outcome is that the increases in global power (CON) and long-range synchrony (FPN) would be more apparent from rest to task. This would further support the proposition that CON is suited to stably lend processing resources, and FPN to adaptively integrate task-specific information. Moreover, possible interactions between the properties discovered herein (Fig. 7) and electrophysiological properties remains an empirical question.

Taken together, constructing a functional cartography by combining multiple measures of large-scale network interactions allowed us to characterize the FPN and CON as complementary systems of cognitive control. We demonstrated that network interactions in both the FPN and CON could reliably predict task rule sets, suggesting their critical role in task representation. Further, we demonstrated that FPN regions enacted control via flexible coordination of reconfiguring connectivity patterns, and CON regions enacted control via flexible switching of network affiliations to lend resources to task-relevant networks. These results corroborated prior neurocognitive theories that distinct mechanisms of cognitive control are instantiated in parallel via separate large-scale brain systems. Looking forward, we expect the dynamic network neuroscience approach expanded upon here will be effective for functionally characterizing the relationship between neural and cognitive dynamics in other brain systems and other cognitive paradigms.

References

Amelio, A., & Tagarelli, A. (2017). Revisiting Resolution and Inter-Layer Coupling Factors in Modularity for Multilayer Networks. *arXiv [cs.SI]*. Retrieved from http://arxiv.org/abs/1709.07253

Anderson, ML., & Magruder, J. (2017). Split-Sample Strategies for Avoiding False Discoveries. *National Bureau of Economic Research*, Working Papers 23544.

Bassett, DS., Wymbs, NF., Porter, MA., Mucha, PJ., Carlson, JM., & Grafton, ST. (2011). Dynamic reconfiguration of human brain networks during learning. *Proceedings of the National Academy of Sciences of the United States of America*, 108(18), 7641–7646.

Bassett, DS., Porter, MA., Wymbs, NF., Grafton, ST., Carlson, JM., & Mucha, PJ. (2013). Robust detection of dynamic community structure in networks. *Chaos*, *23*(1), 013142.

Bassett, DS., Wymbs, NF., Rombach, MP., Porter, MA., Mucha, PJ., & Grafton, ST. (2013). Task-based core-periphery organization of human brain dynamics. *PLoS Computational Biology*, 9(9), e1003171.

Blair, RC., & Karniski, W. (1993). An alternative method for significance testing of waveform difference potentials. *Psychophysiology*, *30*(5), 518–524.

Botvinick, MM. (2007). Conflict monitoring and decision making: reconciling two perspectives on anterior cingulate function. *Cognitive, Affective & Behavioral Neuroscience*, *7*(4), 356–366.

Botvinick, M., & Braver, T. (2015). Motivation and cognitive control: from behavior to neural mechanism. *Annual Review of Psychology*, *66*, 83–113.

Braem, S., Bugg, JM., Schmidt, JR., Crump, MJC., Weissman, DH., Notebaert, W., & Egner, T. (2019). Measuring Adaptive Control in Conflict Tasks. *Trends in Cognitive Sciences*, *23*(9), 769–783.

Braun, U., Schäfer, A., Walter, H., Erk, S., Romanczuk-Seiferth, N., Haddad, L., …Bassett, DS. (2015). Dynamic reconfiguration of frontal brain networks during executive cognition in humans. *Proceedings of the National Academy of Sciences of the United States of America*, *112*(37), 11678–11683.

Chen, M., Kuzmin, K., & Szymanski, BK. (2015, July 2). Community Detection via Maximization of Modularity and Its Variants. *arXiv* [physics.soc-ph].

Cohen, MR., & Maunsell, JHR. (2009). Attention improves performance primarily by reducing interneuronal correlations. *Nature Neuroscience*, *12*(12), 1594–1600.

Cole, MW., Bagic, A., Kass, R., & Schneider, W. (2010). Prefrontal dynamics underlying rapid instructed task learning reverse with practice. *The Journal of Neuroscience: The Official Journal of the Society for Neuroscience*, *30*(42), 14245–14254.

Cole, MW., Bassett, DS., Power, JD., Braver, TS., & Petersen, SE. (2014). Intrinsic and task-evoked network architectures of the human brain. *Neuron*, 83(1), 238–251.

Cole, MW., Braver, TS., & Meiran, N. (2017). The task novelty paradox: Flexible control of inflexible neural pathways during rapid instructed task learning. *Neuroscience and Biobehavioral Reviews*, *81*(Pt A), 4–15.

Cole, MW., Ito, T., Schultz, D., Mill, R., Chen, R., & Cocuzza, C. (2019). Task activations produce spurious but systematic inflation of task functional connectivity estimates. *NeuroImage*, *189*, 1–18.

Cole, MW., Laurent, P., & Stocco, A. (2013). Rapid instructed task learning: a new window into the human brain's unique capacity for flexible cognitive control. *Cognitive, Affective & Behavioral Neuroscience,* 13(1), 1–22.

Cole, MW., Reynolds, JR., Power, JD., Repovs, G., Anticevic, A., & Braver, TS. (2013). Multi-task connectivity reveals flexible hubs for adaptive task control. *Nature Neuroscience*, 16(9), 1348–1355.

Cole, MW., & Schneider, W. (2007). The cognitive control network: Integrated cortical regions with dissociable functions. *NeuroImage*, *37*(1), 343–360.

Cole, MW., Yeung, N., Freiwald, WA., & Botvinick, M. (2009). Cingulate cortex: diverging data from humans and monkeys. *Trends in Neurosciences*, *32*(11), 566–574.

Crittenden, BM., Mitchell, DJ., & Duncan, J. (2016). Task Encoding across the Multiple Demand Cortex Is Consistent with a Frontoparietal and Cingulo-Opercular Dual Networks Distinction. *The Journal of Neuroscience: The Official Journal of the Society for Neuroscience*, *36*(23), 6147–6155.

Desimone, R., & Duncan, J. (1995). Neural mechanisms of selective visual attention. *Annual Review of Neuroscience*, *18*, 193–222.

Desimone, R., Wessinger, M., Thomas, L., & Schneider, W. (1990). Attentional control of visual perception: cortical and subcortical mechanisms. *Cold Spring Harbor Symposia on Quantitative Biology*, *55*, 963–971.

Dosenbach, NUF., Fair, DA., Cohen, AL., Schlaggar, BL., & Petersen, SE. (2008). A dual-networks architecture of top-down control. *Trends in Cognitive Sciences*, 12(3).

Dosenbach, NUF., Fair, DA., Miezin, FM., Cohen, AL., Wenger, KK., Dosenbach, RA. T., …Petersen, SE. (2007). Distinct brain networks for adaptive and stable task control in humans. *Proceedings of the National Academy of Sciences of the United States of America*, *104*(26), 11073–11078.

Dosenbach, NUF., Visscher, KM., Palmer, ED., Miezin, FM., Wenger, KK., Kang, HC., … Petersen, SE. (2006). A core system for the implementation of task sets. *Neuron*, *50*(5), 799–812.

Feldman, J. (2013). The neural binding problem(s). *Cognitive Neurodynamics*, *7*(1), 1–11.

Fox, MD., Snyder, AZ., Vincent, JL., Corbetta M., Van Essen DC., Raichle ME. (2005). The human brain is intrinsically organized into dynamic, anticorrelated, functional networks. *Proceedings of the National Academy of Sciences of the United States of America*, 102(27), 9673-9678.

Fuster, JM., Bauer, RH., & Jervey, JP. (1985). Functional interactions between inferotemporal and prefrontal cortex in a cognitive task. *Brain Research*, *330*(2), 299–307.

Gershon, RC., Wagster, MV., Hendrie, HC., Fox, NA., Cook, KF., & Nowinski, CJ. (2013). NIH toolbox for assessment of neurological and behavioral function. *Neurology*, *80*(11 Suppl 3), S2–S6.

Glasser, MF., Coalson, TS., Robinson, EC., Hacker, CD., Harwell, J., Yacoub, E., … Van Essen, DC. (2016). A multi-modal parcellation of human cerebral cortex. *Nature*, 536(7615), 171–178.

Glasser, MF., Sotiropoulos, SN., Wilson, JA., Coalson, TS., Fischl, JL., Andersson, J., … Jenkinson, M. (2013). The minimal preprocessing pipelines for the Human Connectome Projects. *NeuroImage* 80, 105–124.

Glerean, E., Pan, RK., Salmi, J., Kujala, R., Lahnakoski, J. M., Roine, U., … Jääskeläinen, I. P. (2016). Reorganization of functionally connected brain subnetworks in high-functioning autism. *Human Brain Mapping*, *37*(3), 1066–1079.

Gordon, EM., Laumann, TO., Adeyemo, B., Huckins, JF., Kelley, WM., & Petersen, SE. (2016). Generation and Evaluation of a Cortical Area Parcellation from Resting-State Correlations. *Cerebral Cortex*, *26*(1), 288–303.

Guimerà, R., & Amaral, LAN. (2005). Cartography of complex networks: modules and universal roles. *Journal of Statistical Mechanics*, 2005(P02001), nihpa35573.

Haxby, JV., Gobbini, MI., Furey, ML., Ishai, A., Schouten, JL., & Pietrini, P. (2001). Distributed and overlapping representations of faces and objects in ventral temporal cortex. *Science*, *293*(5539), 2425–2430.

He, BJ. (2013). Spontaneous and task-evoked brain activity negatively interact. *The Journal of Neuroscience: The Official Journal of the Society for Neuroscience*, *33*(11), 4672–4682.

Ito, T., Brincat, SL., Siegel, M., Mill, RD., He, BJ., Miller, EK., Rotstein, HG., & Cole, MW. (2019). Task-evoked activity quenches neural correlations and variability in large-scale brain systems. In *bioRxiv* (p. 560730). https://doi.org/10.1101/560730

Ito, T., Kulkarni, KR., Schultz, DH., Mill, RD., Chen, RH., Solomyak, LI., & Cole, MW. (2017). Cognitive task information is transferred between brain regions via resting-state network topology. *Nature Communications*, 8(1), 1027.

Ji, J. L., Spronk, M., Kulkarni, K., Repovš, G., Anticevic, A., & Cole, M. W. (2019). Mapping the human brain's cortical-subcortical functional network organization. *NeuroImage*, *185*, 35–57.

Koenigs, M., Young, L., Adolphs, R., Tranel, D., Cushman, F., Hauser, M., & Damasio, A. (2007). Damage to the prefrontal cortex increases utilitarian moral judgements. *Nature*, *446*(7138), 908–911.

Krienen, FM., Yeo, BTT., & Buckner, RL. (2014). Reconfigurable task-dependent functional coupling modes cluster around a core functional architecture. *Philosophical Transactions of the Royal Society of London. Series B, Biological Sciences*, *369*(1653).

Mantel, N. (1967). The detection of disease clustering and a generalized regression approach. *Cancer Research*, *27*(2), 209–220.

Marcus, D.S., Harwell, J., Olsen T., Hodge, M., Glasser, M.F., Prior, F., Jenkinson, M., Laumann, T., Curtiss, S.W., Van Essen, D.C. (2011) Informatics and data mining tools and strategies for the Human Connectome Project. Frontiers in Neuroinformatics 5:4.

Mattar, MG., Cole, MW., Thompson-Schill, SL., & Bassett, DS. (2015). A Functional Cartography of Cognitive Systems. *PLoS Computational Biology*, 11(12), e1004533.

Medaglia, JD., Lynall, ME., & Bassett, DS. (2015). Cognitive network neuroscience. *Journal of Cognitive Neuroscience*, *27*(8), 1471–1491.

Miller, EK., & Cohen, JD. (2001). An integrative theory of prefrontal cortex function. *Annual Review of Neuroscience*, 24.

Mucha, PJ., Richardson, T., Macon, K., Porter, MA., & Onnela, JP. (2010). Community structure in time-dependent, multiscale, and multiplex networks. *Science*, 328(5980).

Mur, M., Bandettini, PA., & Kriegeskorte, N. (2009). Revealing representational content with pattern-information fMRI--an introductory guide. *Social Cognitive and Affective Neuroscience*, *4*(1), 101–109.

Murphy, K., Birn, RM., Handwerker, DA., Jones, TB., & Bandettini, PA. (2009). The impact of global signal regression on resting state correlations: are anti-correlated networks introduced? *NeuroImage*, *44*(3), 893–905.

Nichols, TE., & Holmes, AP. (2002). Nonparametric permutation tests for functional neuroimaging: a primer with examples. *Human Brain Mapping*, *15*(1), 1–25.

Ponce-Alvarez, A., He, BJ., Hagmann, P., & Deco, G. (2015). Task-Driven Activity Reduces the Cortical Activity Space of the Brain: Experiment and Whole-Brain Modeling. *PLoS Computational Biology*, *11*(8), e1004445.

Power, JD., Cohen, AL., Nelson, SM., Wig, GS., Barnes, KA., Church, JA., … Petersen, SE. (2011). Functional network organization of the human brain. *Neuron*, *72*(4), 665–678.

Power, JD., Schlaggar, BL., Lessov-Schlaggar, CN., & Petersen, SE. (2013). Evidence for hubs in human functional brain networks. *Neuron*, 79(4), 798–813.

Roy, M., Shohamy, D., & Wager, TD. (2012). Ventromedial prefrontal-subcortical systems and the generation of affective meaning. *Trends in Cognitive Sciences*, *16*(3), 147–156.

Sadaghiani, S., & D'Esposito, M. (2015). Functional Characterization of the Cingulo-Opercular Network in the Maintenance of Tonic Alertness. *Cerebral Cortex*, *25*(9), 2763–2773.

Sadaghiani, S., Scheeringa, R., Lehongre, K., Morillon, B., Giraud, AL., & Kleinschmidt, A. (2010). Intrinsic connectivity networks, alpha oscillations, and tonic alertness: a simultaneous electroencephalography/functional magnetic resonance imaging study. *The Journal of Neuroscience: The Official Journal of the Society for Neuroscience*, *30*(30), 10243–10250.

Sadaghiani, S., Scheeringa, R., Lehongre, K., Morillon, B., Giraud, AL., D'Esposito, M., & Kleinschmidt, A. (2012). α-band phase synchrony is related to activity in the fronto-parietal adaptive control network. *The Journal of Neuroscience: The Official Journal of the Society for Neuroscience*, *32*(41), 14305–14310.

Schneider, W., & Chein, JM. (2003). Controlled & automatic processing: behavior, theory, and biological mechanisms. *Cognitive Science*, *27*(3), 525–559.

Schneider, W., Eschman, A., Zuccolotto, A. E-Prime: User's guide (Psychology Software Incorporated, 2002).

Schultz, DH., Ito, T., Solomyak, LI., Chen, RH., Mill, RD., Anticevic, A., & Cole, MW. (2019). Global connectivity of the frontoparietal cognitive control network is related to depression symptoms in the general population. *Network Neuroscience*. Advance publication.

Seamans, JK., & Yang, CR. (2004). The principal features and mechanisms of dopamine modulation in the prefrontal cortex. *Progress in Neurobiology*, *74*(1), 1–58.

Seeley WW, Menon V, Schatzberg AF, Keller J, Glover GH, Kenna H, Reiss AL, Greicius MD. (2007). Dissociable intrinsic connectivity networks for salience processing and executive control. *J Neurosci*. 27:2349–2356.

Sporns, O., & Betzel, R. (2016). Modular Brain Networks. *Ann. Review of Psychology*, 67, 613-640.

Vaden, KI., Jr, Kuchinsky, SE., Cute, SL., Ahlstrom, JB., Dubno, JR., & Eckert, MA. (2013). The cingulo-opercular network provides word-recognition benefit. *The Journal of Neuroscience: The Official Journal of the Society for Neuroscience*, *33*(48), 18979–18986.

Varoquaux, G., Raamana, PR., Engemann, DA., Hoyos-Idrobo, A., Schwartz, Y., & Thirion, B. (2017). Assessing and tuning brain decoders: Cross-validation, caveats, and guidelines. *NeuroImage*, *145*(Pt B), 166–179.

Waskom, ML., Kumaran, D., Gordon, AM., Rissman, J., & Wagner, AD. (2014). Frontoparietal representations of task context support the flexible control of goal-directed cognition. *The Journal of Neuroscience: The Official Journal of the Society for Neuroscience*, *34*(32), 10743–10755.

Yeo, BTT., Krienen, FM., Sepulcre, J., Sabuncu, MR., Lashkari, D., Hollinshead, M., … Buckner, RL. (2011). The organization of the human cerebral cortex estimated by intrinsic functional connectivity. *Journal of Neurophysiology*, *106*(3), 1125–1165.

Yeo, BTT., Krienen, FM., Eickhoff, SB., Yaakub, SN., Fox, PT., Buckner, RL., … Chee, MWL. (2015). Functional Specialization and Flexibility in Human Association Cortex. *Cerebral Cortex*, *25*(10), 3654–3672.

Supplement

Table 1-1. Demographic characteristics of the discovery dataset (n=50).

	Male (n=19)				Female (n=31)				
	n	%	mean*	SD (+/-)	n	%	mean*	SD (+/-)	test (male vs female)**
Age (years)			21.16	2.93			19.90	1.64	t(25)=1.71, *p*=0.10
18-24	17	89.47			31	100.00			
25-34	2	10.53			0	0.00			
35-44	0	0.00			0	0.00			
Ethnicity/Race			White	n/a			Black	n/a	χ^2 (5, N=50)=6.29, *p*=0.18
American Indian or Alaskan Native	0	0.00			0	0.00			
Asian	5	26.32			10	32.26			
Black or African American	3	15.79			12	38.71			
Hispanic or Latino	4	21.05			2	6.45			
Native Hawaiin or Pacific Islander	0	0.00			0	0.00			
White or Caucasian	7	36.84			6	19.35			
Other	0	0.0			1	3.23			
Education			student	n/a			student	n/a	χ^2 (2, N=50)=1.27, *p*=0.26
Some college/Associate's degree	15	78.95			28	90.32			
College/Graduate degree	4	21.05			3	9.68			
Not reported	0	0.00			0	0.00			

Table 1-1. Demographic data (discovery dataset, n=50). There were no significant differences between identified genders on the distributions of age, ethnicity, or education.
* The measure of center used for categorical variables was the mode. 'Student' refers to 'some college'.
** Testing significant differences between males and females. Age: this was a two-sample t-test (adjusted for unequal sample sizes); Ethnicity/race and education: this was a chi-square test of independence.

Table 1-2. Demographic characteristics of the replication dataset (n=50).

	Male (n=25)				Female (n=25)				
	n	%	mean*	SD (+/-)	n	%	mean*	SD (+/-)	test (male vs female)**
Age (years)			25.00	5.35			23.16	3.52	t(48)=1.44, *p*=0.16
18-24	12	48.00			17	68.00			
25-34	10	40.00			8	32.00			
35-44	3	12.00			0	0.00			
Ethnicity/Race			Asian	n/a			Asian	n/a	χ^2 (5, N=50)=7.23, *p*=0.30
American Indian or Alaskan Native	3	12.00			0	0.00			
Asian	8	32.00			10	40.00			
Black or African American	5	20.00			3	12.00			
Hispanic or Latino	1	4.00			4	16.00			
Native Hawaiin or Pacific Islander	0	0.00			0	0.00			
White or Caucasian	7	28.00			8	32.00			
Other	1	4.00			0	0.00			
Education			graduate	n/a			student	n/a	χ^2 (2, N=50)=1.47, *p*=0.48
Some college/Associate's degree	9	36.00			12	48.00			
College/Graduate degree	13	52.00			12	48.00			
Not reported	3	12.00			1	4.00			

Table 1-2. Demographic data (replication dataset, n=50). All table features are the same as Table 1-1. Note that there were no significant differences between identified genders on the distributions of age, ethnicity, or education.

Table 4-1. Similarities of resting-state FC and multitask FC.

C-PRO Rule-Set	Correlation with Rest (*Mantel-r*)	Shared Variance (R^2)
Sensory rules		
Vertical orientation	0.7966	0.6346
Red color	0.7918	0.6269
High pitch sound	0.7964	0.6343
Constant tone	0.7864	0.6184
Motor rules		
Left index finger	0.7847	0.6158
Right index finger	0.7966	0.6346
Left middle finger	0.7939	0.6303
Right middle finger	0.7844	0.6153
Logic rules		
Both	0.7983	0.6373
Either	0.7934	0.6295
Not both	0.7833	0.6136
Neither	0.7966	0.6346

Table 4-1. Relationships between intrinsic rsFC and tFC estimates via Mantel-r. tFC data was based on each of the 12 C-PRO rules (see Fig. 1), averaged across n=50 participants.

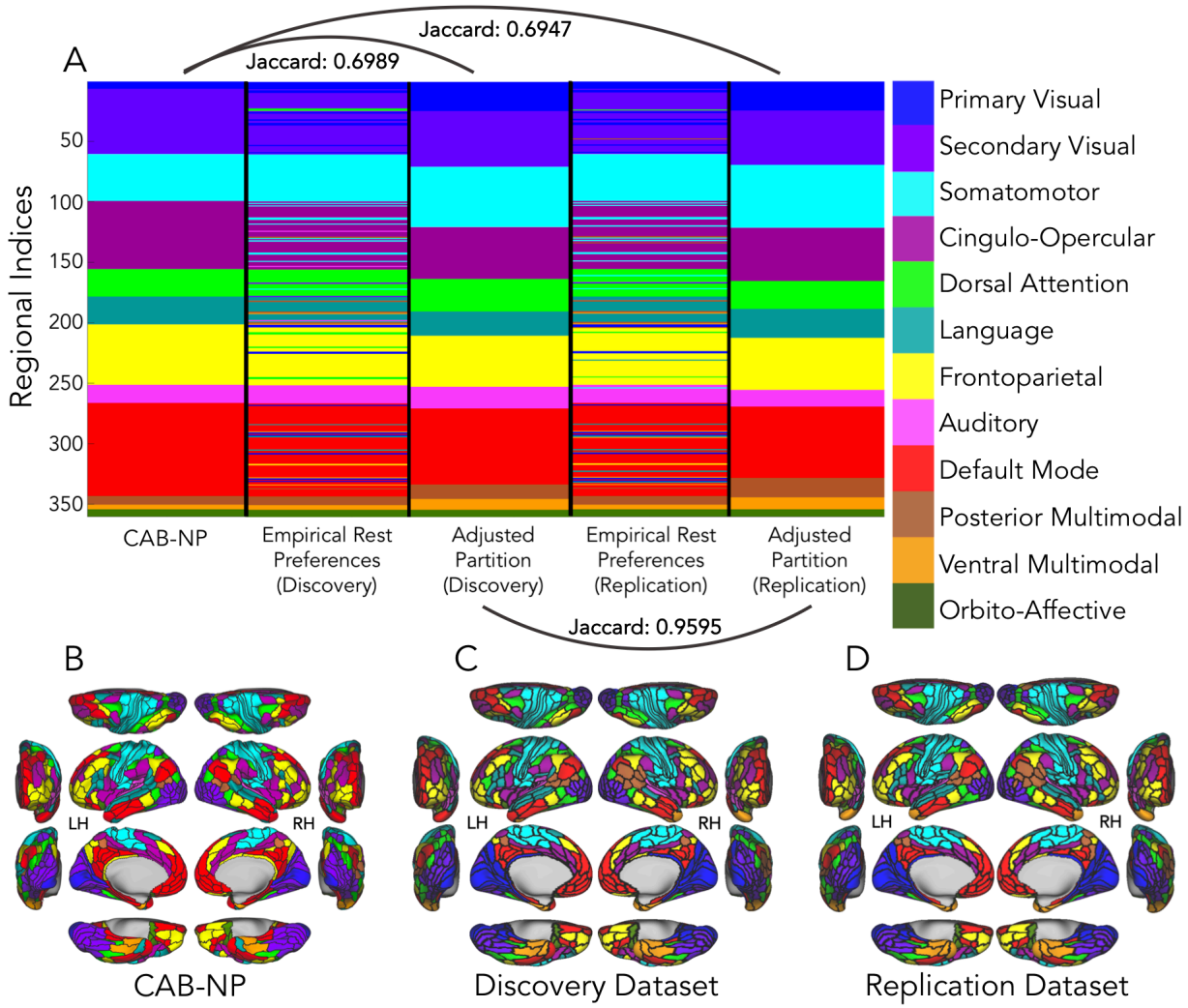

Figure 4-1. The Cole-Anticevic brain-wide network partition (CAB-NP) adjusted by empirical resting-state FC data (Fig. 4A), for both the discovery dataset (n=50) and the replication dataset (n=50). (***A***) Regional (y-axis; Glasser et al., 2016 parcels) assignments are color-coded according to the CAB-NP (rightmost scale; and as in Fig. 4C). The CAB-NP column depicts the original resting-state network partition by Ji et al. (2019). The empirically-derived rest preferences are shown, unordered, for both the discovery and replication datasets, as well as their ordered counterparts (i.e., "adjusted partitions"). These adjusted partitions were used for all analyses (see Materials and Methods for details). (***B***) CAB-NP by Ji et al. (2019) projected onto brain regions. (***C***) The empirically-adjusted CAB-NP for the discovery dataset projected onto brain regions. The Jaccard similarity coefficient between the CAB-NP and the empirically-adjusted discovery set partition was 0.6989. (***D***) The empirically-adjusted CAB-NP for the replication dataset projected onto brain regions. The Jaccard similarity coefficient between discovery and replication partitions was 0.9595, suggesting the partition method used herein will have high external validity. The Jaccard similarity coefficient between the CAB-NP and the empirically-adjusted replication set partition was 0.6947. This suggests a relatively high similarity between each of the empirically-adjusted partitions (discovery and replication) and the CAB-NP. The least similarity was observed in the primary visual network, which was expanded to include CAB-NP secondary visual and dorsal attention regions in the empirical adjustments.

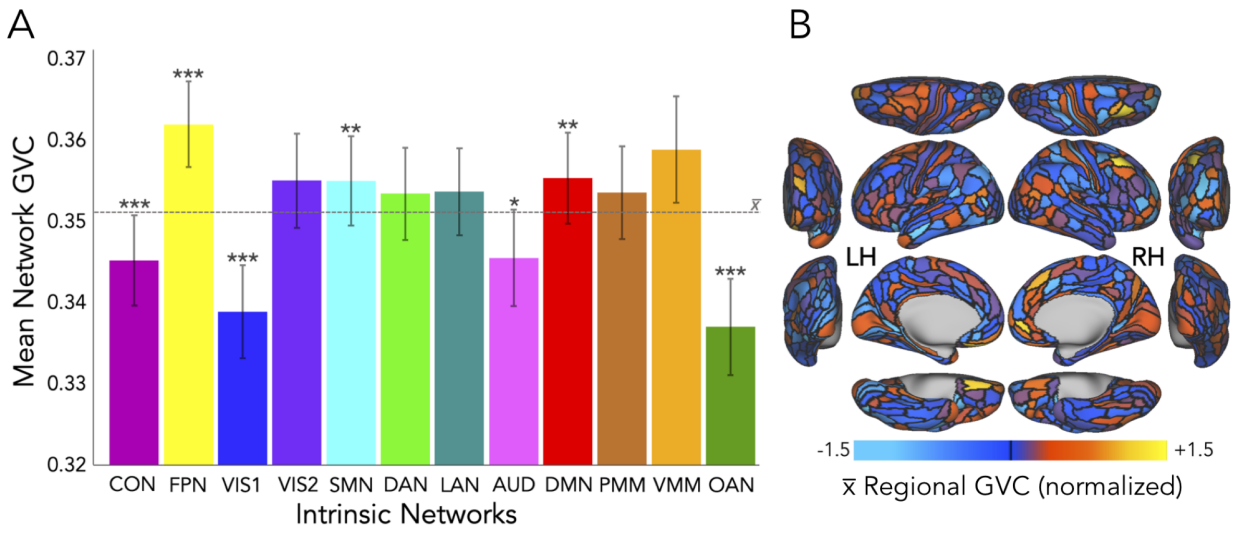

Figure 5-1. Global variability coefficient (GVC), replication dataset. (***A-B***) Panels are represented exactly as in Fig. 5, except measurements were taken for the replication dataset (n=50).

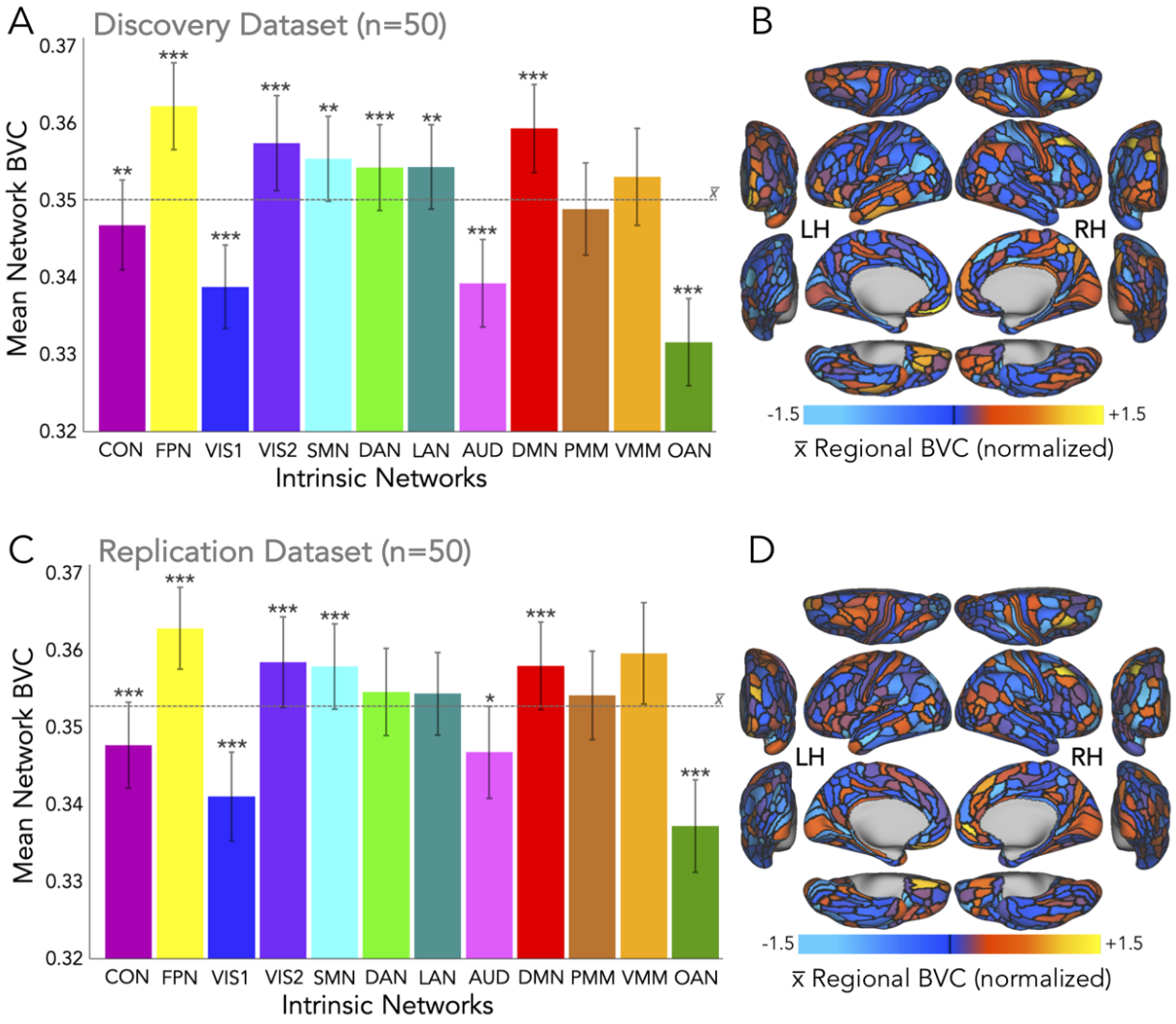

Figure 5-2. Between-network variability coefficient (BVC) data. (***A-B***) Panels are represented exactly as in Fig. 5 (GVC), except for BVC (discovery dataset, n=50). (***C-D***) Same as in A-B, except for the replication dataset (n=50).

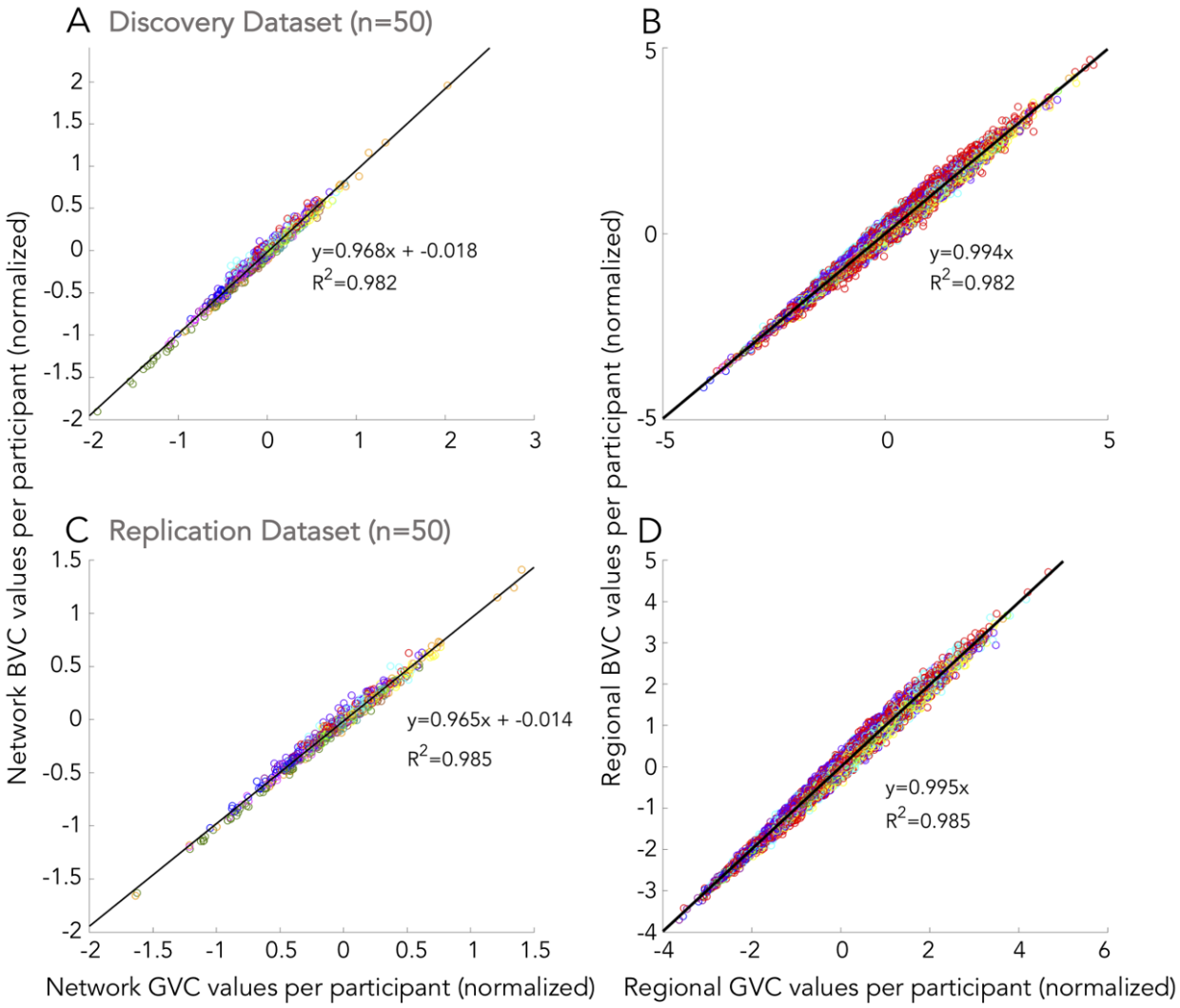

Figure 5-3. Data demonstrating the linear relationships between GVC and BVC. In each panel, circles represent individual participant's scores (i.e., what was averaged in Fig. 5), color-coded for network assignments (as in Fig. 4C). Slope-intercept formulae are listed ($y = mx + b$), along with shared variances (R^2). At all levels of measurement and for both discovery and replication sets, GVC and BVC were highly correlated. (***A***) Discovery dataset (n=50), network-level. (***B***) Discovery dataset, regional-level. (***C***) Replication dataset (n=50), network-level. (***D***) Replication dataset, regional level.

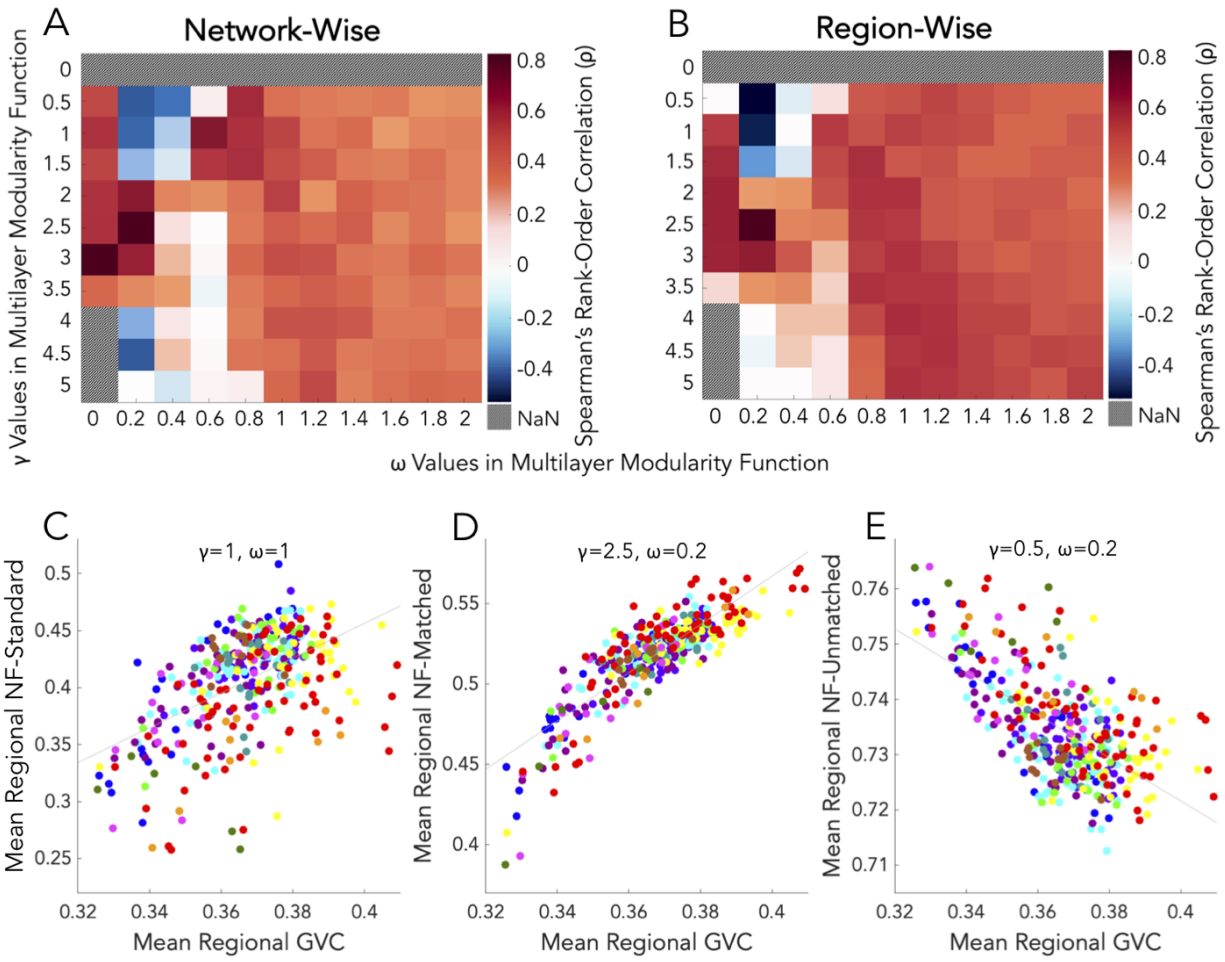

Figure 5-4. Data comparing global variability coefficient (GVC) with network flexibility (NF), discovery dataset (n=50). (***A***) Network-wise comparisons (Spearman's rank order correlation) of GVC and NF sweeped by multilayer modularity parameters, across participants. (***B***) Same as A, but at the region-wise level. (***C***) Regional mean GVC plotted over regional mean NF-standard (multilayer modularity parameters: γ=1 and ω=1). NF-standard results were yielded by the standard parameter combination. Each region (mean across N=50 participants) was plotted as individual scatter points, and color-coded according to the network it belongs to (as in Fig. 4C). (***D***) Same as C, but with NF-matched represented on the y-axis (γ=2.5 and ω=0.2). This parameter combination yielded NF results most correlated with GVC (or, "matched"), as depicted in A and B by dark red squares. (***E***) Same as C and D, but with NF-unmatched represented on the y-axis (γ=0.5 and ω=0.2). This parameter combination yielded NF results least correlated with GVC (or, "unmatched"), as depicted in A and B by blue squares. The inconsistency of this result with the results in panels C-E suggested the need for a new measure of network switching that was less dependent on parameter selection.

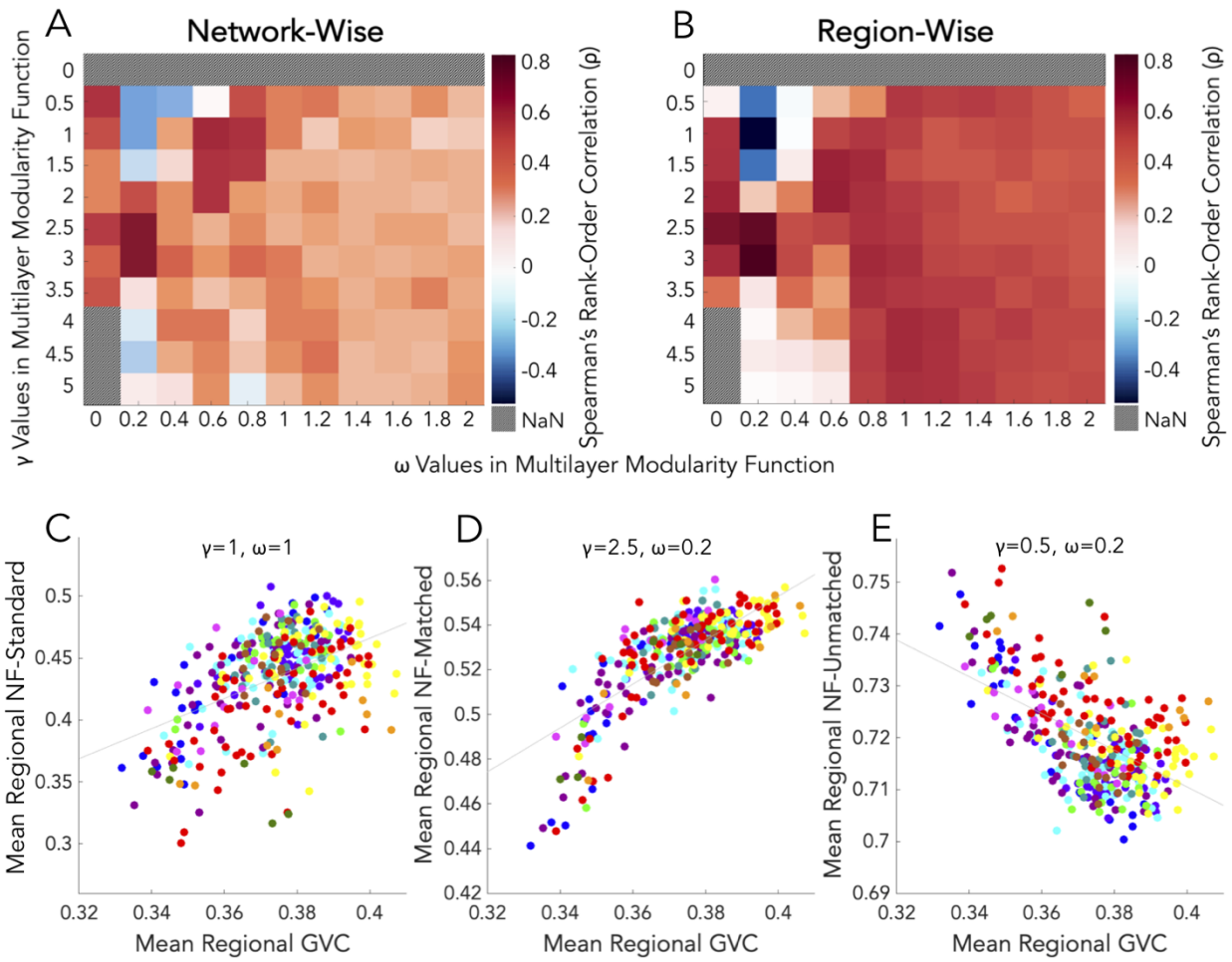

Figure 5-5. Data comparing GVC with NF, replication dataset (n=50). (***A-F***) Panels are represented exactly as in Fig. 5-4 (discovery dataset, n=50), except measurements were taken for the replication dataset (n=50). Note that the parameter combination utilized for NF-standard (γ=1 and ω=1) (panel C) was the same as in Fig. 5-4C because this was based on the literature-standard. The parameter combinations used in the multilayer modularity function yielding NF-matched (panel D) and NF-unmatched (panel E) were set to the same values as in Fig. 5-4 even though there were higher and lower Rho values in the region-wise comparison with GVC for the replication set (panel B), respectively. More specifically, the regional NF vector most similar to GVC was yielded by γ=3 and ω=0.2 in the replication dataset, as opposed to γ=2.5 and ω=0.2 in the discovery dataset. However, γ=2.5 and ω=0.2 did yield the highest Rho value in the network-wise comparison with GVC (panel A) in the replication set, thus we continued to use this combination for NF-matched as it lead to the highest similarity score in most analyses. The same rationale was applied to NF-unmatched, where the parameter combination of γ=0.5 and ω=0.2 was used.

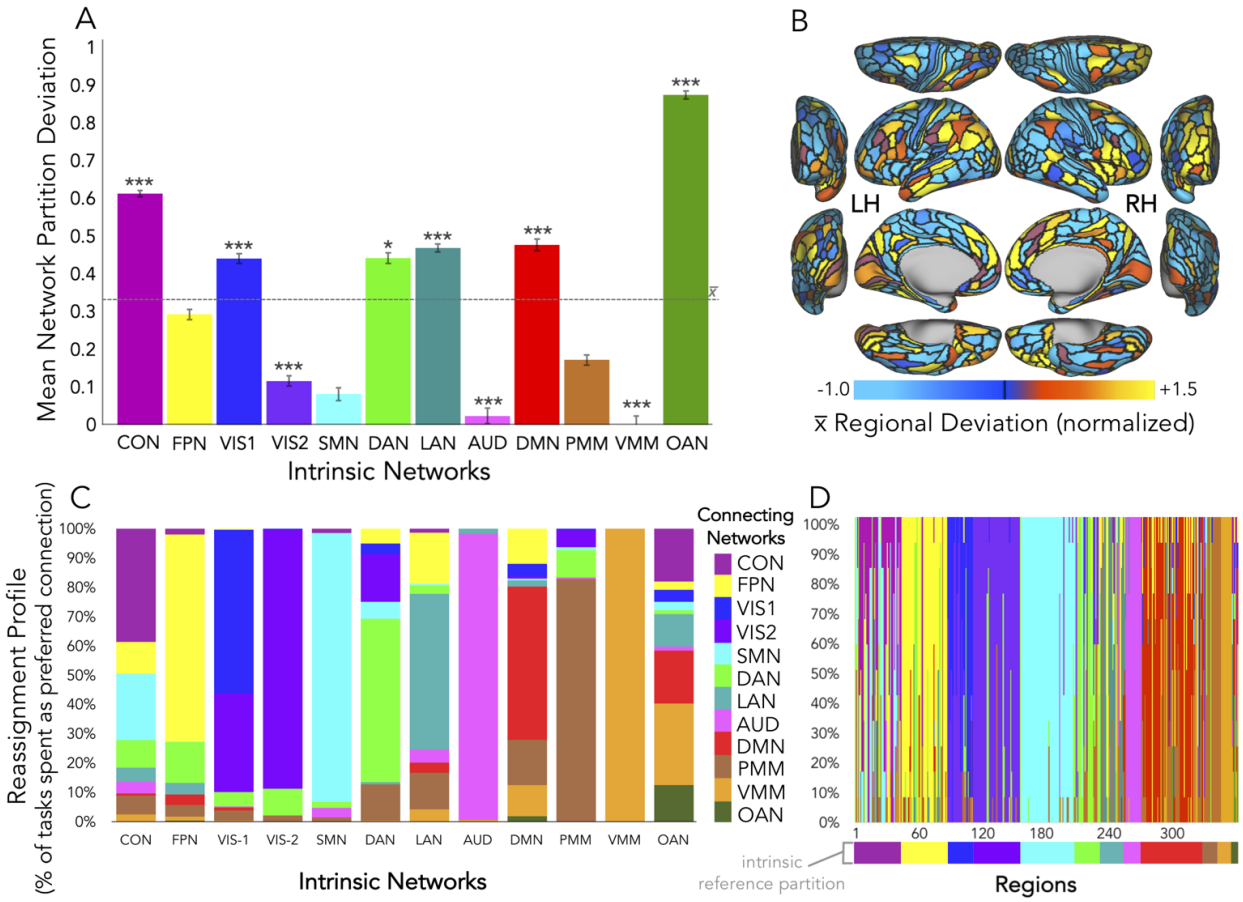

Figure 6-1. Network partition deviation and reassignment profiles, replication dataset. (***A-D***) Panels are represented exactly as in Fig. 6, except measurements were taken for the replication dataset (n=50).

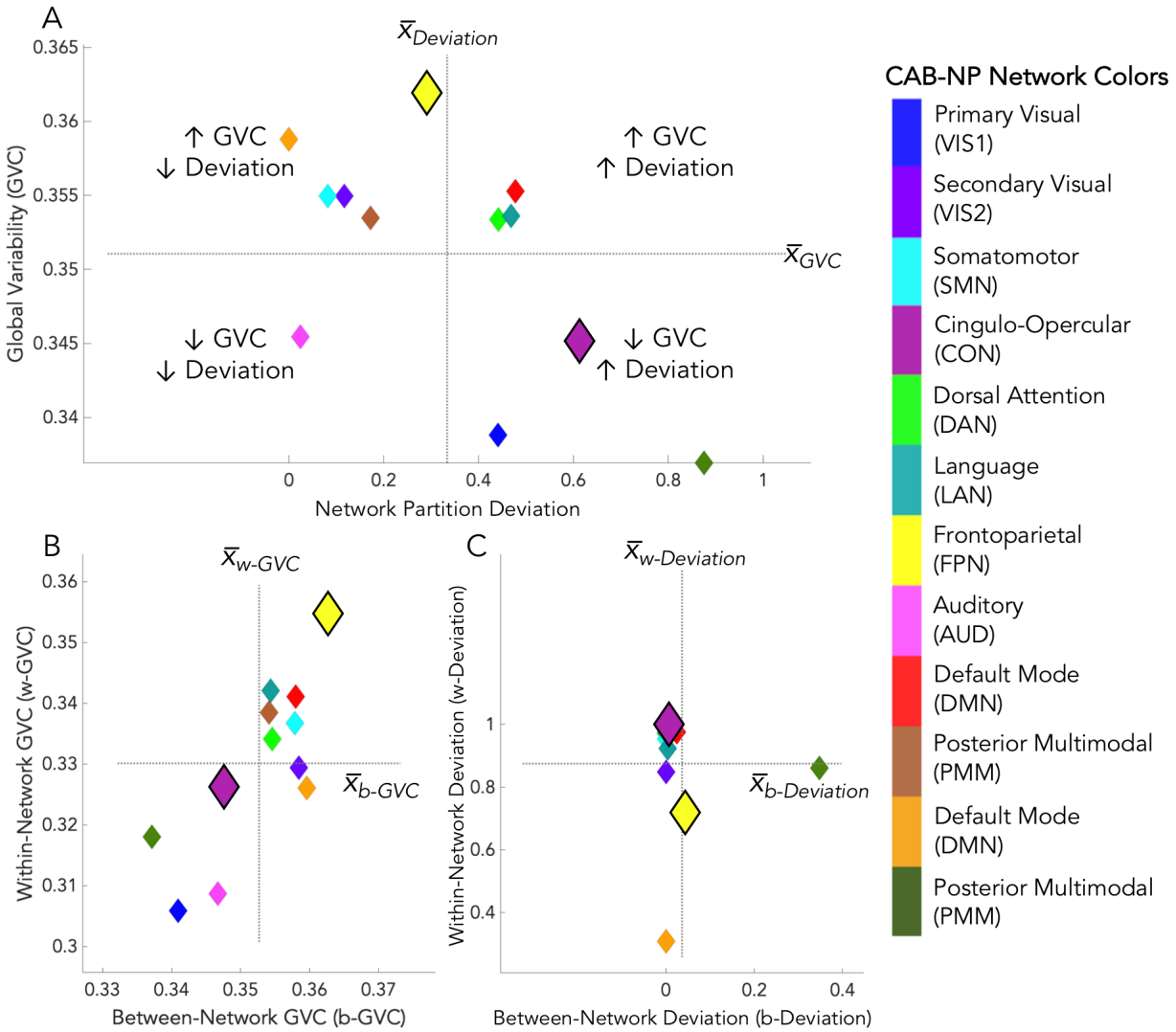

Figure 7-1. Cognitive control cartographies, replication dataset. (***A-C***) Panels are represented exactly as in Fig. 7, except measurements were taken for the replication dataset (n=50). The far-right legend depicts the CAB-NP color scheme (as in Fig. 4C) used for the diamonds.

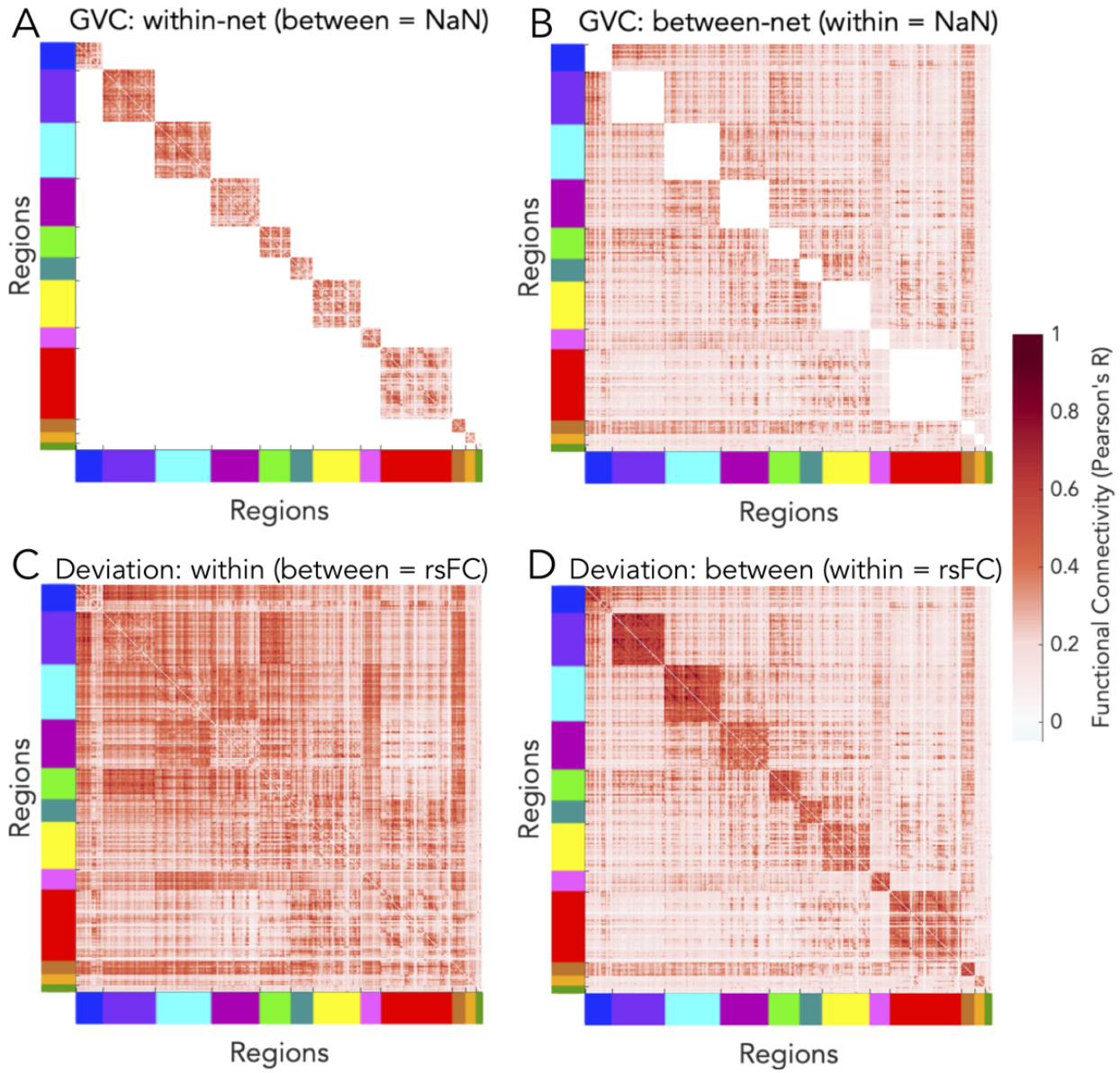

Figure 7-2. Input data schemes used in computing measures of the secondary cognitive control cartographies (Fig. 7B and 7C). Data refers to functional connectivity estimates (Pearson's R; colored according to the right-most scale). Put another way, each panel contains modified correlation matrices. The cross-state means are visually represented, but analyses included all 64 C-PRO task states. Axes are color coded according to the empirically-adjusted CAB-NP (see Fig. 4C). (***A***) Representation of input data for within-network GVC (Fig. 7B, y-axis). Between-network FC estimates were set to 'NaN' (white). (***B***) Input data for between-network GVC (Fig. 7B, x-axis). Within-network FC estimates were set to 'NaN' (white). (***C***) Input data for within-network deviation (Fig. 7C, y-axis). Between-network FC estimates were set to their resting-state values. (***D***) Input data for between-network deviation (Fig. 7C, x-axis). Within-network FC estimates were set to their resting-state values.

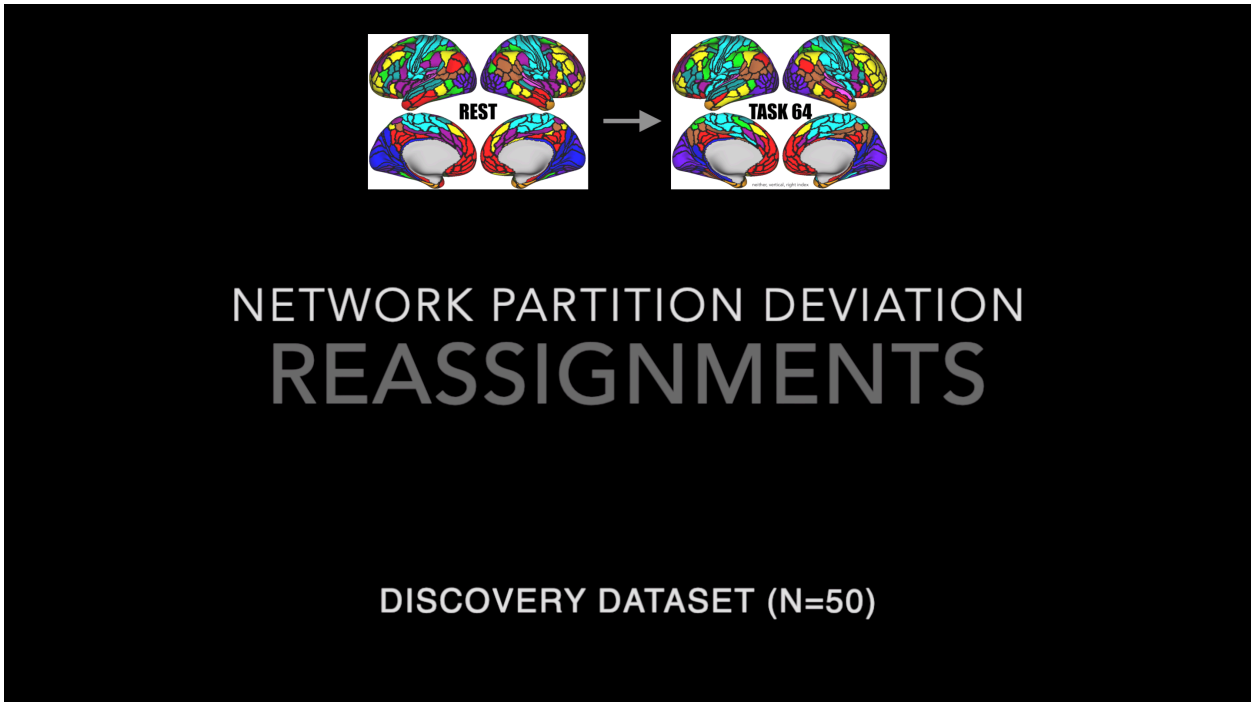

Multimedia 1. *Preview image for Multimedia, video 1.* Video of each region's network "preference" observed during the computation of network partition deviation, across all 64 C-PRO task states, and for n=50 discovery dataset participants (see Materials and Methods). Briefly, per task state and region, the maximum connectivity estimate was found, and its location relative to the predefined partition (empirically adjusted CAB-NP) was indexed (see Fig. 3B and Table 1). These network indices were then mapped back onto brain schematics to visualize how deviation defines network reassignment across tasks. This video also depicts the dynamics captured by deviation. Some patches of cortex remained stable in their network assignments across states (such as primary and secondary visual networks, shown mainly in occipital regions as blue and purple, respectively). However, some regions and/or networks reassigned with more frequency, such as the shifts in cingulo-opercular preference. The goal of deviation was to quantify these patterns in a systematic manner. Cortical regions on each brain schematic represent the Glasser parcellation scheme (2016), and colors correspond to the CAB-NP naming system (Ji et al., 2019) (see Fig. 4C).

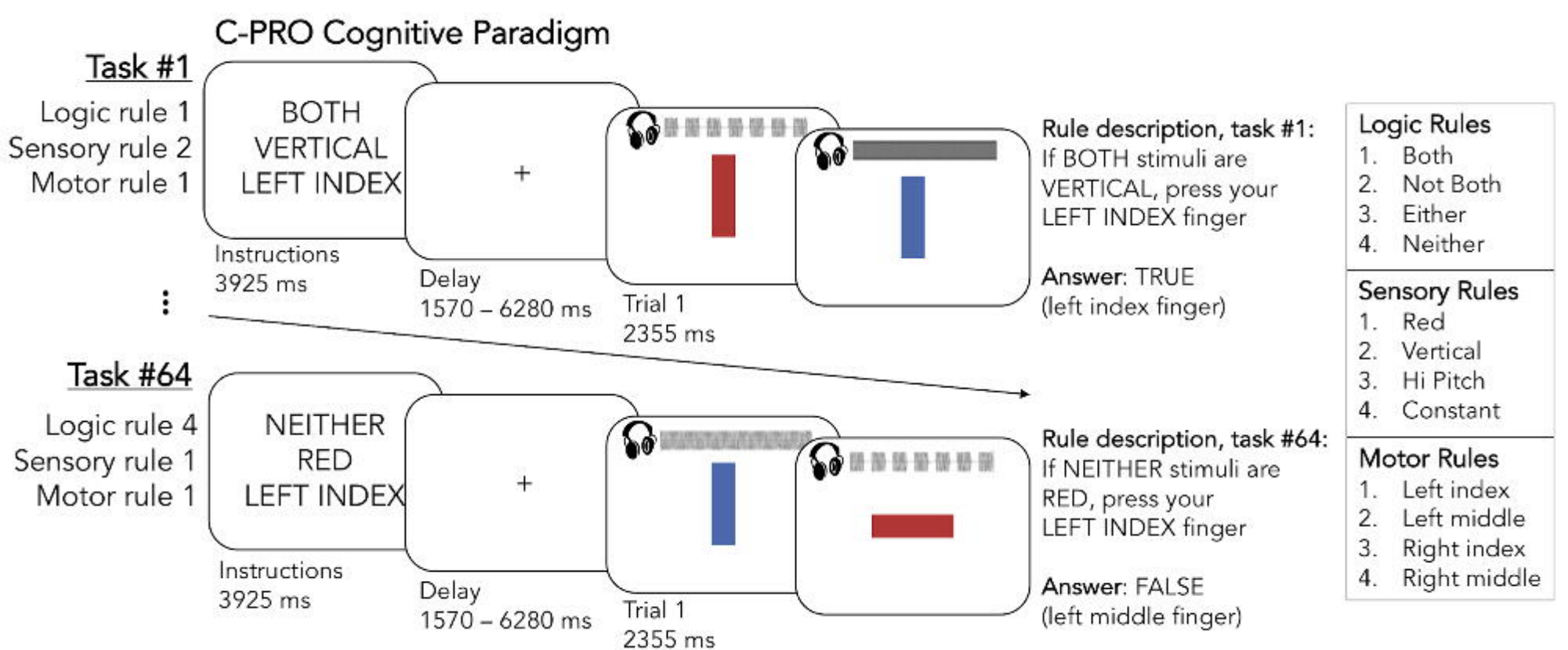
C-PRO Cognitive Paradigm
Task #1
Logic rule 1
Sensory rule 2
Motor rule 1
BOTH
VERTICAL
LEFT INDEX
Instructions
3925 ms
+
Delay
1570 – 6280 ms
Trial 1
2355 ms
Rule description, task #1:
If BOTH stimuli are VERTICAL, press your LEFT INDEX finger
Answer: TRUE
(left index finger)
Task #64
Logic rule 4
Sensory rule 1
Motor rule 1
NEITHER
RED
LEFT INDEX
Instructions
3925 ms
+
Delay
1570 – 6280 ms
Trial 1
2355 ms
Rule description, task #64:
If NEITHER stimuli are RED, press your LEFT INDEX finger
Answer: FALSE
(left middle finger)
Logic Rules
1. Both
2. Not Both
3. Either
4. Neither
Sensory Rules
1. Red
2. Vertical
3. Hi Pitch
4. Constant
Motor Rules
1. Left index
2. Left middle
3. Right index
4. Right middle

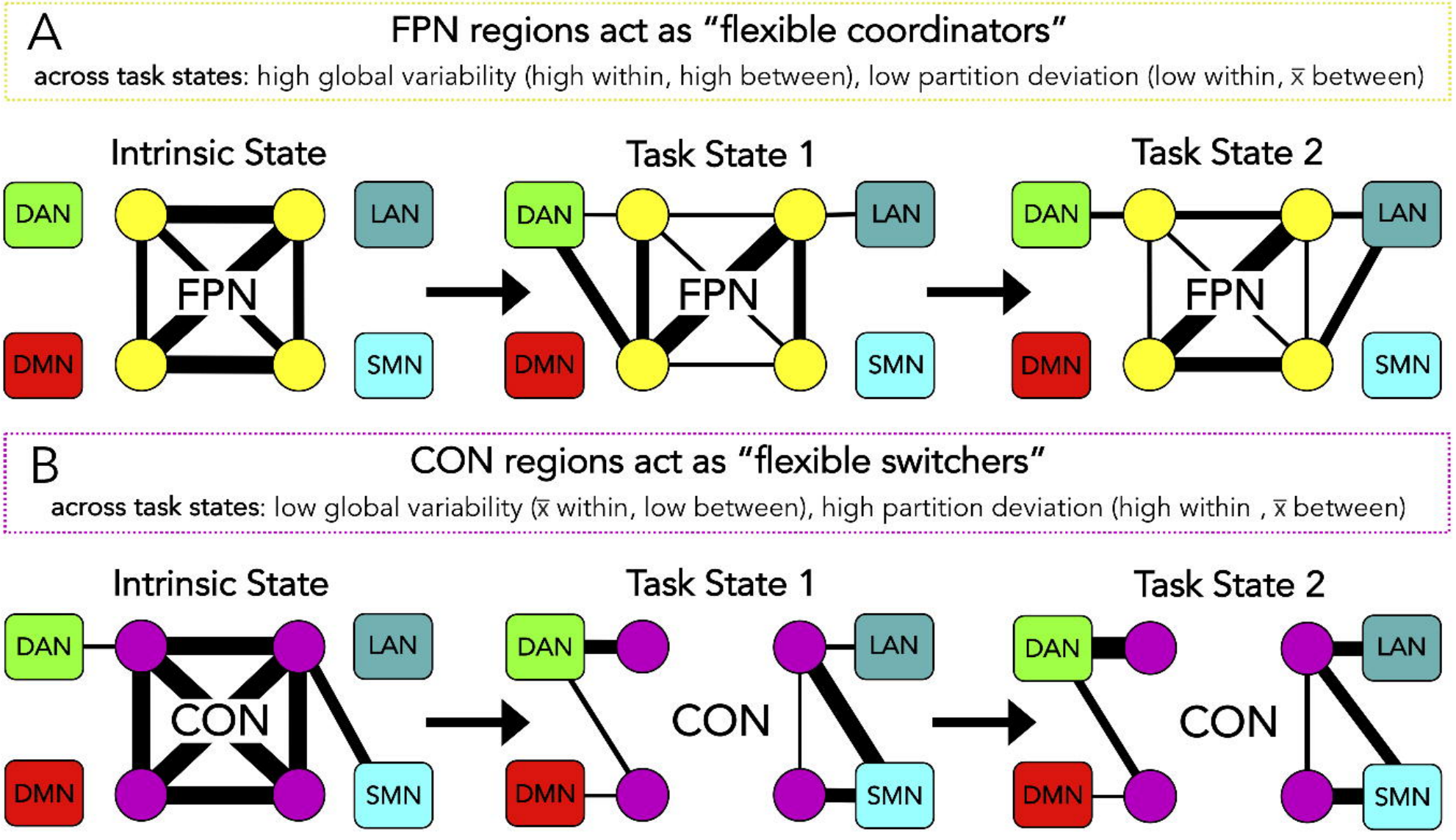
A
FPN regions act as "flexible coordinators"
across task states: high global variability (high within, high between), low partition deviation (low within, x̄ between)
Intrinsic State
Task State 1
Task State 2
DAN
LAN
DMN
SMN
FPN
B
CON regions act as "flexible switchers"
across task states: low global variability (x̄ within, low between), high partition deviation (high within , x̄ between)
CON

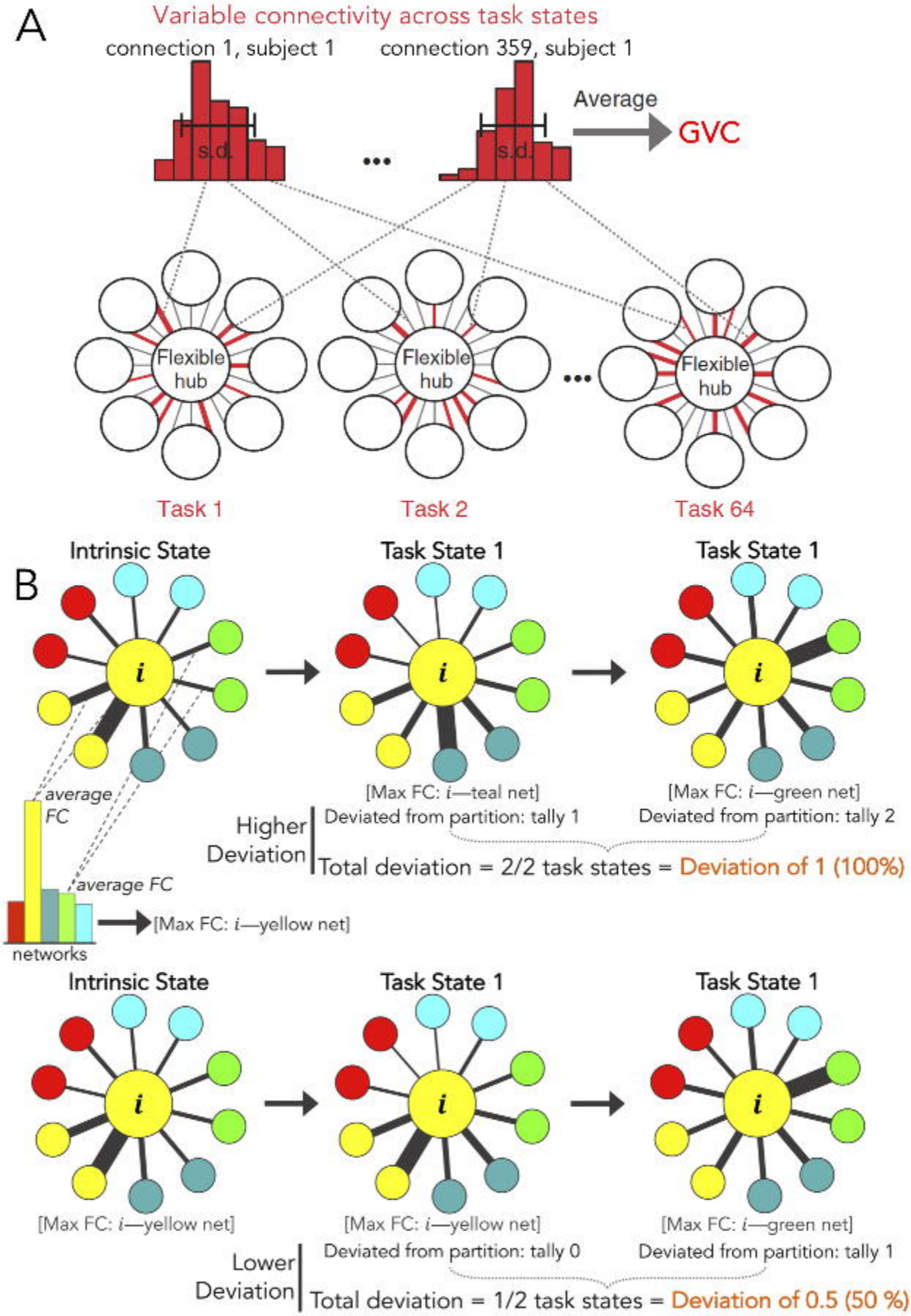
A
Variable connectivity across task states
connection 1, subject 1
connection 359, subject 1
s.d.
s.d.
Average
GVC
Flexible hub
Flexible hub
Flexible hub
Task 1
Task 2
Task 64
B
Intrinsic State
Task State 1
Task State 1
i
i
i
average FC
average FC
networks
[Max FC: i—yellow net]
[Max FC: i—teal net]
Deviated from partition: tally 1
[Max FC: i—green net]
Deviated from partition: tally 2
Higher Deviation
Total deviation = 2/2 task states = Deviation of 1 (100%)
Intrinsic State
Task State 1
Task State 1
i
i
i
[Max FC: i—yellow net]
[Max FC: i—yellow net]
Deviated from partition: tally 0
[Max FC: i—green net]
Deviated from partition: tally 1
Lower Deviation
Total deviation = 1/2 task states = Deviation of 0.5 (50 %)

Table 1. Graph theoretical diagnostic metrics for network reconfiguration properties across states.

Metric name	Formula	Measures; Diagnoses	Parameter-space?	Relies on a pre-defined partition?
Global Variability Coefficient (GVC)	$GVC_n = \frac{1}{N}\sum_{i=1}^{n}\sqrt{\frac{\sum_{l=1}^{T}(FC_{il} - \bar{x}_{FCl})^2}{T-1}}$	Variable FC across tasks; flexible hubs	No	No
Between-Network Variability Coefficient (BVC)	$BVC_n = \frac{1}{N'}\sum_{i'=1}^{n'}\sqrt{\frac{\sum_{l=1}^{T}(FC_{i'l} - \bar{x}_{FCl'})^2}{T-1}}$	Variable FC across tasks, between-network; flexible hubs	No	Yes
Network Partition Deviation (Deviation)	$Deviation_n = 1 - \left[\frac{\sum_{j=1}^{T}\left[\left(\max\left(\frac{\sum_{rS=1}^{c} FC_{cj}}{C}\right)\right) \in rS\right]}{T}\right]$	Network preference changes over time, compared to intrinsic partition; reassignment profile	Minimal	Yes

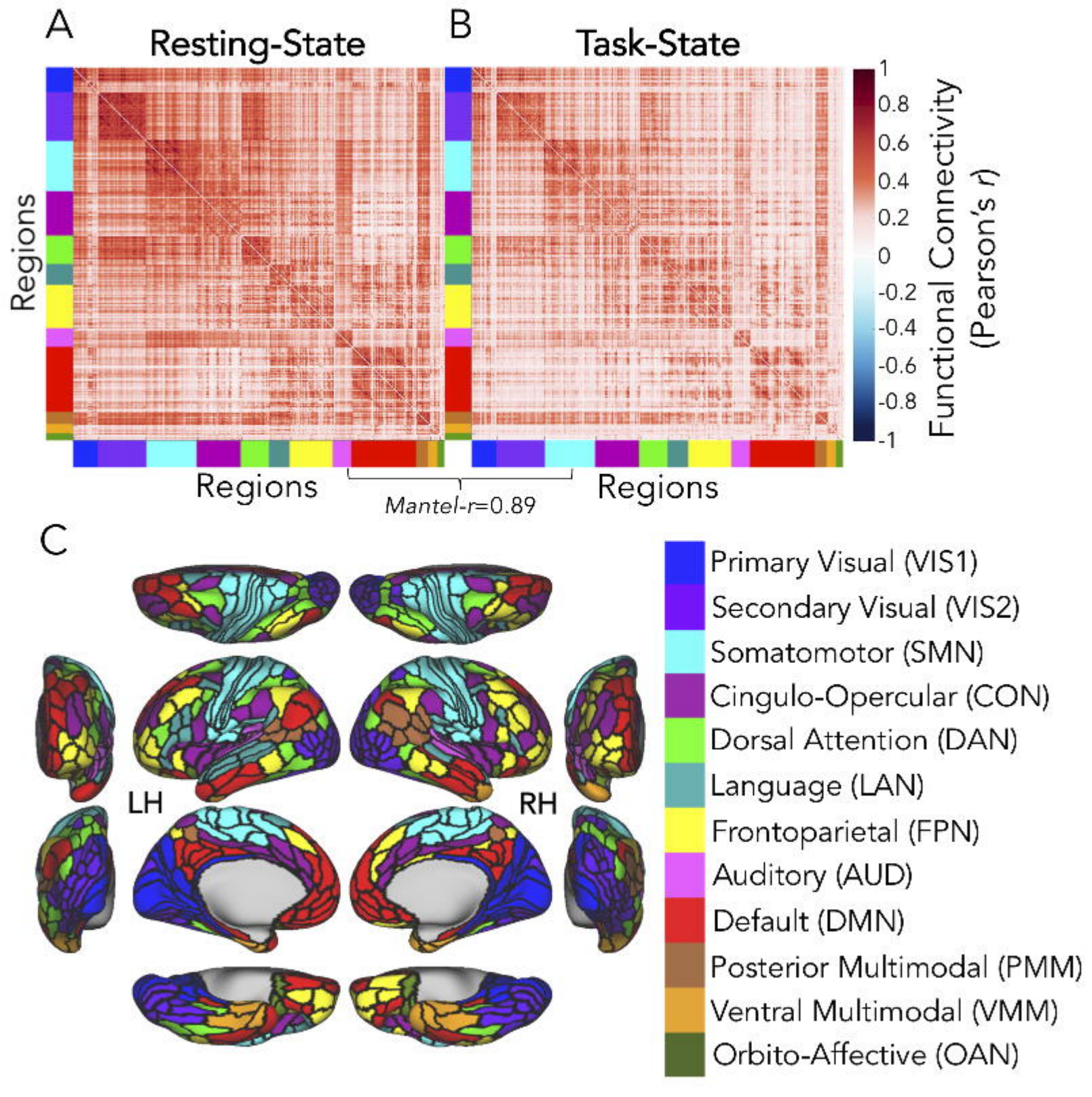
A
Resting-State
B
Task-State
Regions
Regions
Regions
Mantel-r=0.89
1
0.8
0.6
0.4
0.2
0
-0.2
-0.4
-0.6
-0.8
-1
Functional Connectivity
(Pearson's r)
C
LH
RH
Primary Visual (VIS1)
Secondary Visual (VIS2)
Somatomotor (SMN)
Cingulo-Opercular (CON)
Dorsal Attention (DAN)
Language (LAN)
Frontoparietal (FPN)
Auditory (AUD)
Default (DMN)
Posterior Multimodal (PMM)
Ventral Multimodal (VMM)
Orbito-Affective (OAN)

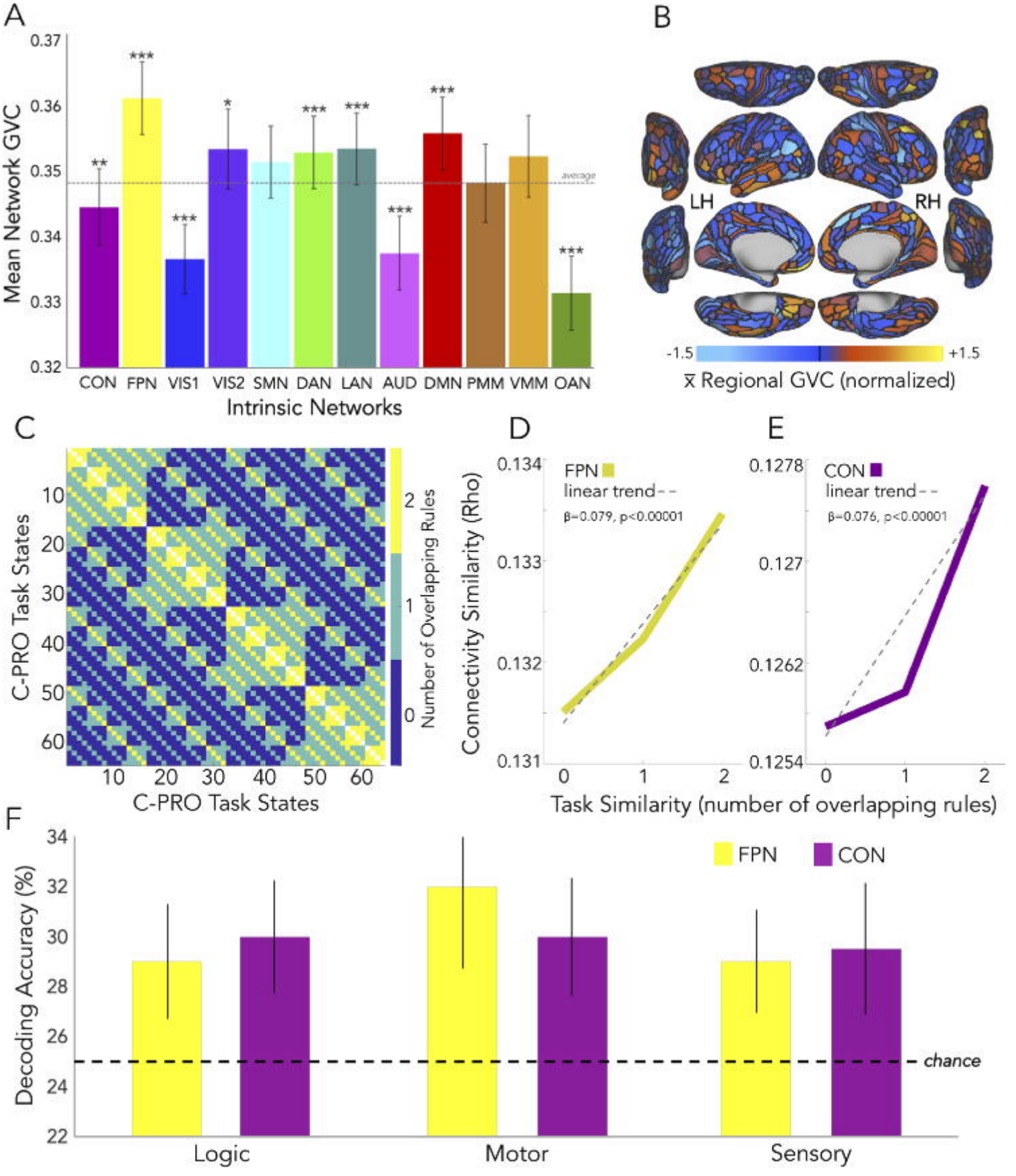
A
Mean Network GVC
0.37
0.36
0.35
0.34
0.33
0.32
average
CON FPN VIS1 VIS2 SMN DAN LAN AUD DMN PMM VMM OAN
Intrinsic Networks
B
LH
RH
-1.5
+1.5
x̄ Regional GVC (normalized)
C
C-PRO Task States
Number of Overlapping Rules
D
FPN
linear trend
β=0.079, p<0.00001
Connectivity Similarity (Rho)
0.134
0.133
0.132
0.131
E
CON
linear trend
β=0.076, p<0.00001
0.1278
0.127
0.1262
0.1254
Task Similarity (number of overlapping rules)
F
Decoding Accuracy (%)
FPN
CON
chance
Logic
Motor
Sensory

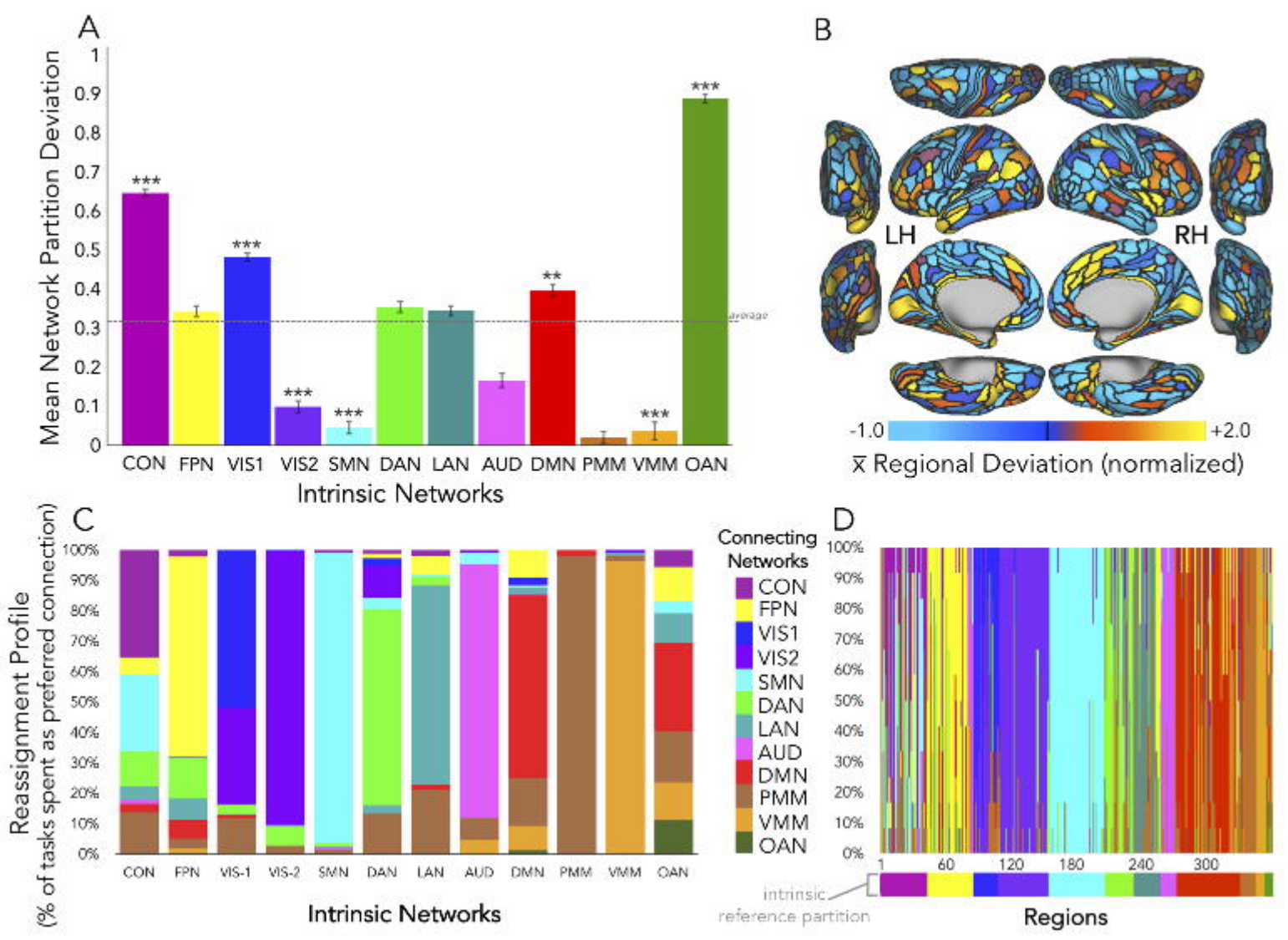
A
Mean Network Partition Deviation
1
0.9
0.8
0.7
0.6
0.5
0.4
0.3
0.2
0.1
0
***
***
***
***
**
***
***
average
CON FPN VIS1 VIS2 SMN DAN LAN AUD DMN PMM VMM OAN
Intrinsic Networks
B
LH
RH
-1.0
+2.0
x̄ Regional Deviation (normalized)
C
Reassignment Profile
(% of tasks spent as preferred connection)
100%
90%
80%
70%
60%
50%
40%
30%
20%
10%
0%
CON FPN VIS-1 VIS-2 SMN DAN LAN AUD DMN PMM VMM OAN
Intrinsic Networks
Connecting Networks
CON
FPN
VIS1
VIS2
SMN
DAN
LAN
AUD
DMN
PMM
VMM
OAN
D
100%
90%
80%
70%
60%
50%
40%
30%
20%
10%
0%
1 60 120 180 240 300
intrinsic reference partition
Regions

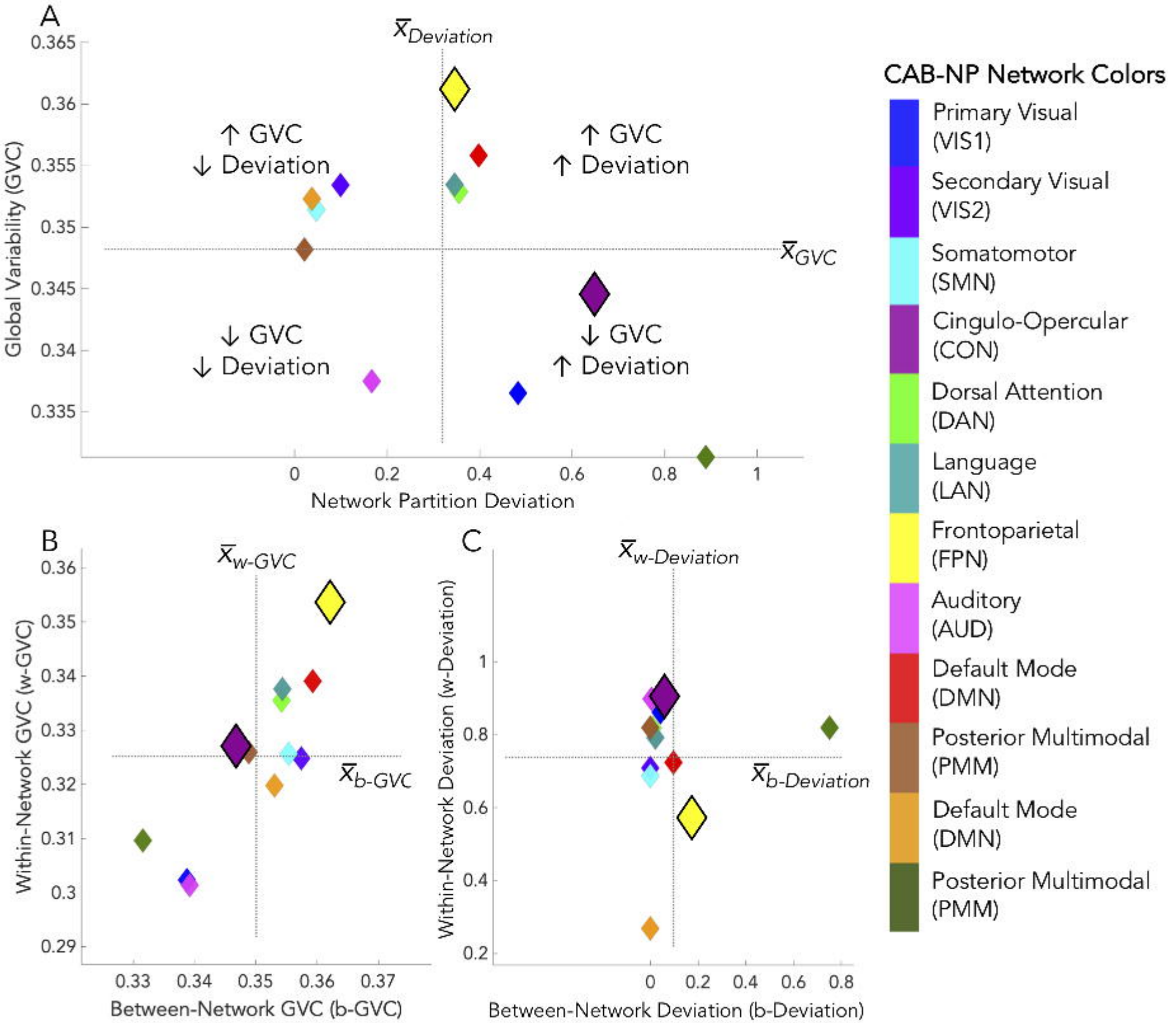
A
$\bar{x}_{Deviation}$
$\bar{x}_{GVC}$
↑ GVC
↓ Deviation
↑ GVC
↑ Deviation
↓ GVC
↓ Deviation
↓ GVC
↑ Deviation
Global Variability (GVC)
Network Partition Deviation
B
$\bar{x}_{w\text{-}GVC}$
$\bar{x}_{b\text{-}GVC}$
Within-Network GVC (w-GVC)
Between-Network GVC (b-GVC)
C
$\bar{x}_{w\text{-}Deviation}$
$\bar{x}_{b\text{-}Deviation}$
Within-Network Deviation (w-Deviation)
Between-Network Deviation (b-Deviation)
CAB-NP Network Colors
Primary Visual (VIS1)
Secondary Visual (VIS2)
Somatomotor (SMN)
Cingulo-Opercular (CON)
Dorsal Attention (DAN)
Language (LAN)
Frontoparietal (FPN)
Auditory (AUD)
Default Mode (DMN)
Posterior Multimodal (PMM)
Default Mode (DMN)
Posterior Multimodal (PMM)

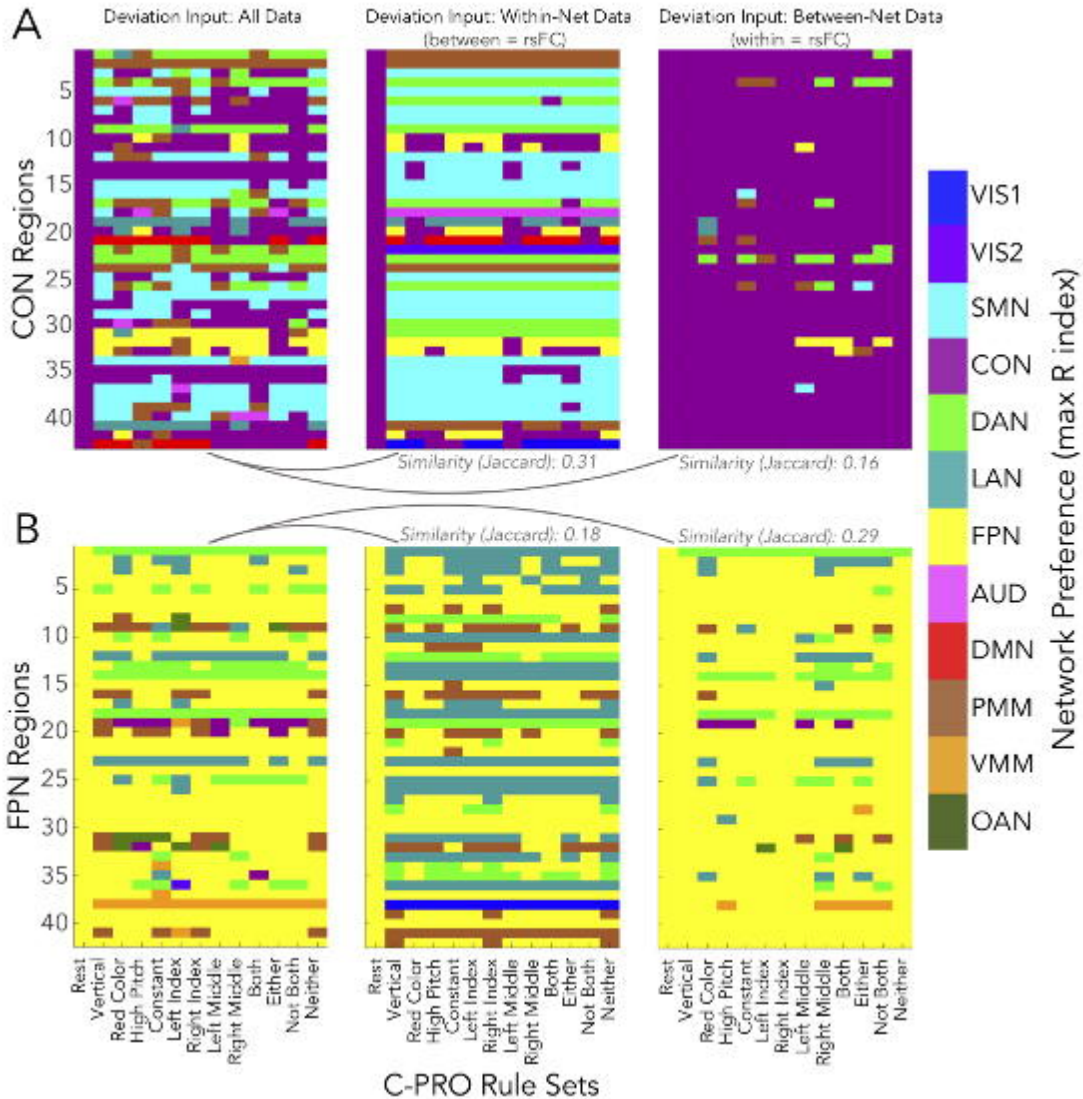
A
Deviation Input: All Data
Deviation Input: Within-Net Data
(between = rsFC)
Deviation Input: Between-Net Data
(within = rsFC)
CON Regions
5
10
15
20
25
30
35
40
Similarity (Jaccard): 0.31
Similarity (Jaccard): 0.16
B
Similarity (Jaccard): 0.18
Similarity (Jaccard): 0.29
FPN Regions
Rest
Vertical
Red Color
High Pitch
Constant
Left Index
Right Index
Left Middle
Right Middle
Both
Either
Not Both
Neither
C-PRO Rule Sets
VIS1
VIS2
SMN
CON
DAN
LAN
FPN
AUD
DMN
PMM
VMM
OAN
Network Preference (max R index)